

# Studies of ERK1/2 with respect to tumor aggressiveness in B16F10 murine melanoma cells

Shuvojit Moulik<sup>1</sup>, Sayantani Karmakar<sup>2</sup>, Asmita Basu<sup>3</sup>,  
Swayambhik Mukherjee<sup>4</sup>, Neeraja R<sup>5</sup>, Amitava Chatterjee<sup>6</sup>

<sup>1</sup>Lead scientist, Research and development, Suraksha Diagnostics Pvt. Ltd, Newtown, Kolkata, West Bengal, India

<sup>2</sup>Research Scientist, Research and development, Suraksha Diagnostics Pvt. Ltd, Newtown, Kolkata, West Bengal, India

<sup>3</sup>Research Intern, CWF Labs: Transdisciplinary Healthcare & Research, Bolpur, West Bengal, India

<sup>4</sup>M.Sc., St. Xavier's college (autonomous), Kolkata, West Bengal, India

<sup>5</sup>Junior research fellow, Cochin University of Science and Technology (CUSAT), Kerala, India

<sup>6</sup>Ex-Deputy Director, Chittaranjan National Cancer Institute (CNCI), Kolkata, West Bengal, India

## Abstract

Melanoma is a very aggressive form of skin cancer, it has the potential to spread from a small sized primary tumor and metastasizes to different locations like lungs, bones, lymph nodes, liver and even brain. Extracellular signal regulated kinase (ERK) molecule present in MAPK pathway plays a major role in different carcinogenic processes like cell migration, cell invasiveness by altering the extracellular matrix (ECM). Cell invasiveness is facilitated by matrix metalloproteins (MMPs) by means of degradation of gelatinase enzyme regulated by a family of receptor proteins called integrins. ECM ligand fibronectin causes increased secretion of MMPs, specially MMP2 and MMP9 facilitating invasiveness and metastasis in cancer cells. This study aims to find the modulatory role of ERK1/2 with respect to tumor aggressiveness on both MMP2 and MMP9 in context of melanoma metastasis and invasion. ERK pathway was downregulated through administration of inhibitors. ERK1/2 siRNA gene silencing the effect on MMP2 and MMP9 was studied. The studies were done in B16F10 melanoma cell line and mice model. Significant changes were found in levels of MMP2 and MMP9 after downregulating the ERK pathway and therefore a correlation between ERK and MMP activities was established. Elucidating these molecular phenomena in melanoma, this result can help in developing and improving targeted cancer therapies with multiple options in drug discovery.

**Keywords:** melanoma, ERK, extracellular matrix, MAPK, matrix metalloprotease, integrins

## INTRODUCTION

Melanoma is a deadly cancer primarily affecting the skin. It accounts for around 4% of all skin malignancies accounting for almost 80% skin cancer-related mortality. Melanoma can spread to any organ, including the lung, liver, lymph nodes, and gastrointestinal tract (Braeuer et al., 2014; Kumar et al., 2020). The tumor microenvironment is rapidly becoming recognized as a major regulator of cancer growth. The extracellular matrix (ECM), a fundamental component of the cancer microenvironment, is in

direct contact with tumor cells and serves as a crucial source of growth, survival, motility, along with angiogenic factors that influence tumor biology and progression. Extracellular signal regulated kinase (ERK) is a key molecule located in the Mitogen activated protein kinase (MAPK) pathway responsible for several cell processes in cancer including cell invasiveness which primarily involves breakdown of ECM. Furthermore, cell adhesion to the ECM activates intracellular signaling pathways that can influence cell cycle progression, migration, and differentiation via integrins and other cell surface receptors. Thus, interactions between tumor cells and the ECM are key modulators of tumor cell metastatic potential (Barkan et al., 2008; Kim et al., 2011; Winkler et al., 2020). Alterations that result in abnormal ERK activation are frequent in human malignancies and can be observed at practically every level of the MAPK pathway (Song et al., 2022). BRaf mutations, notably around codon 600, are present in a wide range of malignancies, including roughly half of all cutaneous melanomas (Chung and Hyun, 2020). In our previous studies, authors investigated the possible role of ERK1/2 in modulating matrix metalloproteinase (MMPs) MMP2 and MMP9 in breast cancer cell lines, suggesting that there might be a direct correlation between ERK1/2 activity and MMP2 and MMP9 since MMPs facilitates cell invasiveness by degrading gelatinase which is again differentially regulated by Integrins, a family of receptors. With current advancement in research, silencing / knockout of certain genes along with substances extracted naturally or chemically synthesized in a laboratory have been shown to cause an influence in tumor aggressiveness. Silencing of MYH9 (Non-muscle myosin IIA heavy chain), WISP1 knockout, also plays important role in cases of tumor progression (Kumar et al., 2020; Deng et al., 2019). Our previous results from the breast cancer cell lines were very interesting with respect to ERK's position in the MAPK signaling (Moulik et al., 2014). Hence it was necessary to actually see whether this role was similar in other cancers like melanoma since ERK also plays an important role in melanoma. 90% melanoma is constitutively active due to mutations in NRas and BRaf. An important factor in metastatic spread of melanoma is its interaction with the various components of ECM (Eble and Niland, 2019; Elgundi et al., 2020). Only transformed melanocytes can survive in dermis and this survival seems to be dependent upon expression of molecules that regulate adhesion and interaction between cells and ECM. Most of these interactions are mediated by a heterodimeric family of proteins, the integrins. Recent references shows that the sustained activation of the Ras/Raf/MEK/ERK pathway is involved in the expression of  $\beta$  3 integrins (Haass et al., 2005; Shain and Bastian, 2016). A common cause of resistance in melanoma to apoptosis was activation of ERK signaling cascade and in particular ERK1 and ERK2. Introduction of activated MAPK kinase into melanocytes resulted in tumorigenesis in nude mice (Czarnecka et al., 2020; Sugiura et al., 2021). Hence the melanoma mouse cell line B16F10 was chosen which when introduced to black mice can induce tumor. The aim of this study is to analyze the role of ERK 1 and 2 with respect to tumor aggressiveness in B16F10 cells and also to assess the dose dependent interdependency between MMP9 and ERK 1/2. The study was also extended in mice model in determining the possible role of phosphorylated ERK (pERK) in MMP9/ MMP2 activity after administration of MEK/ ERK inhibitors.

## MATERIALS AND METHODS

### Materials:

#### Cells and Mice

Murine Melanoma cancer cell line B16F10 was obtained from NCCS, Pune. C57BL/6J mice (6 to 8 weeks old) were obtained from institutional animal house. Throughout the experiments, mice were maintained with free access to pellet food and water in plastic cages at  $21 \pm 2$  °C and kept on a 12 h light-dark cycle.

Animal welfare and experimental procedures were performed strictly in accordance with the care and use of laboratory animals and the related ethical regulations of our institute. All efforts were made to minimize the animal's suffering and to reduce the number of animals used.

### **Cell culture materials**

a. Minimal Essential Medium (GIBCO); b. Dulbecco's Modified Eagle's Medium (GIBCO);  
c. McCoy's 5A medium (GIBCO); d. Fetal bovine serum (Lifetech, Biowhittaker)

### **SDS-PAGE**

a. Acrylamide (Promega); b. Bis Acrylamide (Sigma); c. Tris (Promega); d. Sodium Dodecyl Sulphate (Biogene); e. Ammonium Persulphate (Lifetech); f. Glycine; g. Stain (Coomassie Brilliant Blue); h. Bromophenol Blue; i. Methanol; j. Acetic Acid; k. TEMED

### **Gelatin Zymography**

All the materials of SDS- PAGE and a. Gelatin (Sigma); b. Triton-X (Promega); c. NaCl; d. CaCl<sub>2</sub>; e. Gelatin Sepharose 4B beads (Amersham)

### **Western Blot**

All the materials of SDS-PAGE and

**Primary Antibody:** - anti-phospho-ERK, anti-ERK, anti MMP2, anti MMP9, anti JNK, anti phospho-JNK, anti PI-3K, anti-STAT-3 anti-integrins antibody or as required (Sigma, Promega, Santa Cruz).

**Secondary Antibody:** - 2<sup>nd</sup> Antibody : both monoclonal and polyclonal (Promega/Santa Cruz).

**Substrate-** NBT/BCIP or Femto substrate for ECL (Pierce) NaCl, Tris, Tween -20, Tris, Glycine, Methanol, BSA and Nitrocellulose membrane

### **Invasion Assay**

Millicell inserts (Millipore), Matrigel (BD Biosciences)

### **Methods:**

#### **Cell culture**

Cells were grown and maintained in required medium (MEM, DMEM and RPMI) containing 10% FBS in a CO<sub>2</sub> incubator at 37°C.

#### **Cell Extraction**

Cells were initially grown in required medium supplemented with 10% FBS. The cells were collected from culture flasks by trypsinization and homogenized in cell extraction buffer (Tris-37.5mM, NaCl- 75mM, Triton-X-0.5% and pH adjusted to 7.5) at 15 mins of intervals for 1-1.5 h at 4°C. The cells were then centrifuged at 15000 r.p.m for 10 mins at 4°C. The supernatant was collected and the pellet was discarded and the protein of the extract was estimated by Lowry's Method. (It could also be stored at - 86°C till use).

### **Tissue Extraction**

Tissues were cut into small pieces using forceps and scissors and then centrifuged with small amount of PBS and the supernatant was discarded (to remove blood clots). The tissue was homogenized in Tissue extraction buffer (tris 50mM, NaCl 75mM, SDS 0.01% in 100 ml water) at 15 mins interval for 1-1.5 h at 4°C. The homogenate was centrifuged at 15000 r.p.m for 15 mins at 4°C, supernatant (extract) was collected and pellet was discarded. Extract was stored at -86°C till use.

### **Zymography**

Cells were initially grown in the required medium supplemented with 10% FBS in petri dishes, treated for the stipulated time period in SFCM for 24 hours, and the respective serum-free culture medium (SFCMs) was collected. The culture supernatant was collected by centrifugation at 3000 r.p.m for 5 minutes. The MMPs were separated from SFCM using Gelatin Sepharose 4B beads (75 µl) overnight at 4°C. The beads were washed three times with Tris-buffered saline with Tween-20 (TBST) and suspended in 50 µl of 1X sample buffer (0.075 gm Tris, 0.2 gm SDS in 10 ml water, pH 6.8). The suspension was incubated for 30 minutes at 37°C and then centrifuged at 3000 r.p.m. for 3 minutes. The supernatant was then subjected to zymography on 7.5% SDS-PAGE co-polymerized with 0.1% gelatin. The gel was washed in 2.5% Triton-X-100 for 30 minutes to remove SDS and was then incubated overnight in reaction buffer (50 mM Tris-HCl pH 7, 4.5 mM CaCl<sub>2</sub>, 0.2 M NaCl). After incubation, the gel was stained with 0.5% Coomassie Blue in 30% methanol and 10% glacial acetic acid. The bands were visualized by destaining the gel with water.

### **Immunoprecipitation**

Cells were initially grown in the required medium supplemented with 10% FBS in petri dishes. The respective cells were collected. Cell extraction was carried out using the standard extraction protocol, and the protein content of the extracts was estimated by Lowry's method. Equal amounts of protein were taken and immunoprecipitated from the supernatant using the required primary antibodies and protein-G agarose beads, followed by shaking overnight at 4°C. The resultant immune complex was washed three times in PBS and then subjected to western blotting.

### **Western Blot Assay**

Cells were initially grown in the required medium supplemented with 10% FBS in petri dishes. The respective cells were collected. Cell extraction was carried out using the standard extraction protocol, and the protein content of the extracts was estimated by Lowry's method. Equal amounts of protein were taken and, after boiling with 0.1 volumes of β-mercaptoethanol for 5–8 minutes at 80–90°C, were subjected to electrophoresis on 10% SDS-PAGE. The proteins were transferred onto PVDF membranes by Western Blot at 300 mA for 3 hours. The membranes were blocked with 1% BSA and subsequently washed three times with TBST. The immunoblots were reacted with the required primary antibody. The blots were developed using respective alkaline phosphatase-coupled secondary antibodies, and the color was developed using ECL as the substrate.

### **Cell Invasion assay**

The cell invasion was done according to the protocol of Moulik et al., 2014. 24 well transwell plate

(Corning) with 12 inserts were taken and the lower chamber of each well was poured with 600 ml MEM SFCM. Control and fibronectin treated cells (100,000 cells/insert) were seeded in triplicate on membrane in the upper chamber of the insert. Cells were grown for 24 h and 48 h. After the incubation, media was aspirated out from membrane. SFCMs from lower chambers were collected and centrifuged at 3000 rpm for 3 min. The membranes of the inserts were washed thrice with PBS. Cells were then fixed with 4% formaldehyde solution, followed by washing with PBS. Cells were then stained with Gill's hematoxylin for 10 min. Membranes were thoroughly washed with running water. The upper side of the membranes was scraped with buds; membranes were then cut and mounted with glycerol. The cells migrated through the membrane pore were observed under microscope (Moulik et al., 2014).

### Wound Healing Assay

Cells were grown as a monolayer on culture plates in absence (C) and in presence of 50 $\mu$ g/ml the aflavin at 37°C for 24 h (E). The monolayer was scratched with a sterile pipette tip, followed by washing with SFCM to remove cellular debris. The migration of cells across the wound was observed and photographed at 0 h, 6 h and 24 h, 48 h (Moulik et al., 2014).

### siRNA transfection

Single transfection procedure was followed according to the protocol from (Moulik et al., 2014).

Cells were plates 24 h prior to transfection. The cells were incubated at 37°C for 24 h under 5% CO<sub>2</sub>. After incubation, the plate was with PBS (once), and layer with 1.75 ml OptiMEM. The following mixture was prepared and incubated at room temperature for 5 mins.

Tube 1: siRNA: 100 nM (Stock concentration: is 100  $\mu$ M, siRNA:2 $\mu$ l)

OptiMEM: 198  $\mu$ l

Tube 2: Oligofectamine: 4  $\mu$ l

OptiMEM: 46  $\mu$ l

The content of both the tubes were mixed and incubated for further 30 mins. siRNA-lipid mix on the cells (dropwise with constant swirling) was layered. The plate was incubated at 37 °C for 4 h. Fresh media was added after 4 h incubation and incubate further 24 h. Cells were analyzed according to the experiment.

### Double transfection (combinatorial transfection) procedure

For experiment with two round of siRNA transfection, second round of transfection was done in the similar manner as described above after 24 h of first round of Transfection. Scramble control for siRNA was similarly prepared according to Moulik et al., 2014.

### Constitution of siRNA

Prepare 1X nuclease free siRNA buffer from 5X provided by Dharmacon (use nuclease free water, also provided by Santa Cruz). For 100-nMole siRNA, used 1ml 1X nuclease free siRNA buffer. Aliquots the siRNA and stored at -20°C.

### Statistical Analysis

Descriptive statistical analysis was performed to prepare different frequency tables and to calculate the means with corresponding standard errors. Chi-square test was applied as the measures of associations. Test of proportion was used to find the Standard Normal deviate (Z-values) and corresponding p-values

for the test of differences between different proportions. Paired t-test was used to find the differences in means.

## RESULTS AND DISCUSSION

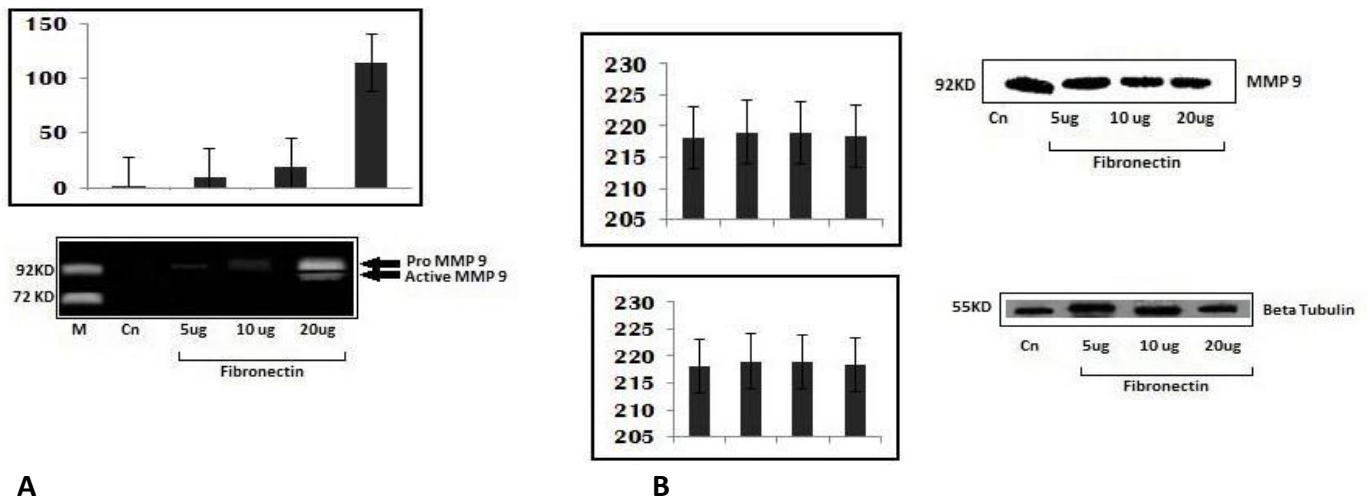


**Figure 1. Effect of fibronectin on the gelatinolytic activity and expression of MMP-9 in B16F10 cells**

**A. Comparative zymographic analysis of MMP-9:** B16F10 cells (300,000 cells/ml) were grown in serum free culture medium in absence (control) and in presence of increasing concentration of Fibronectin (Fn) (5ug/10ug/20ug per ml) for 16 h. Lane M in all zymograms is MMP9 (92 kDa) / MMP-2 (72 KDa) marker lane (SFCM of HT-1080 cells grown for 24 h).

**B. Effect of fibronectin on expression of MMP9 by Immunoblot:** B16F10 cells (300,000 cells/ml) were grown in serum free culture medium in absence (control) and in presence of increasing concentration of Fibronectin (5ug/10ug/20ug per ml) for 16 h. The Fn treated and untreated cells were collected. Cell extraction was carried out using the standard extraction protocol and the protein content of the extracts were estimated by Lowry's method. Equal amount of protein in Lamillie's buffer was taken and subjected to electrophoresis on 8% SDS-PAGE. The proteins were transferred on to PVDF membrane by Western Blot at 50mA for overnight. The membranes were blocked with 4 % BSA and subsequently washed x3 with PBST (phosphate buffer saline and tween 20). The immunoblot were probed for anti-MMP9 antibody. The blots were developed using respective horse redox peroxidase (HRP) coupled second antibodies. The colour was developed using West Femto as substrate.  $\beta$ -tubulin was used as loading control. The accompanying graph represents the comparative densitometric/quantitative analysis of the band intensities using image J Launcher (version 1.4.3.67) and arranged in the similar order as of the lanes. Data are means  $\pm$  SEM of three experiments.

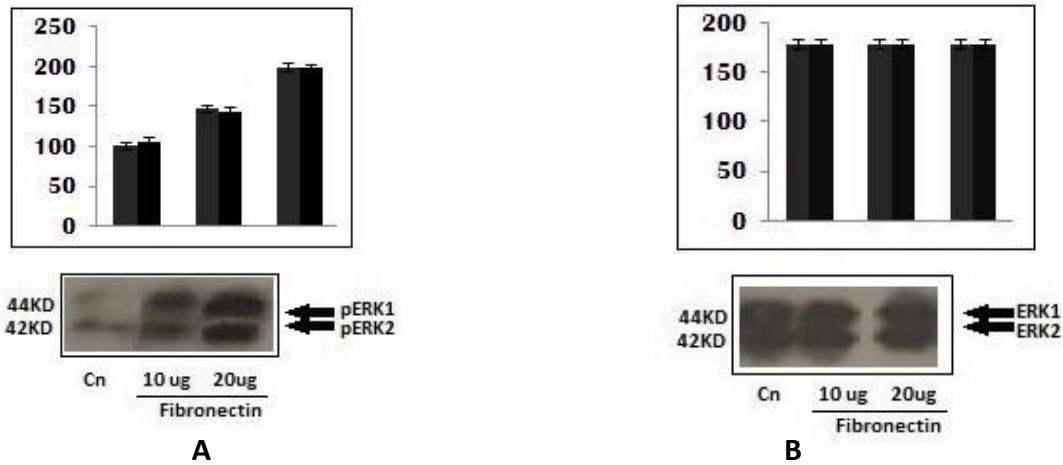


**Figure 2: Effect of fibronectin on expression of pERK/ERK by Immunoblot**

B16F10 cells (300,000 cells/ml) were grown in serum free culture medium in absence (control) and in presence of increasing concentration of Fibronectin (10ug/20ug per ml) for 16 h. The Fn treated and untreated cells were collected. Cell extraction was carried out using the standard extraction protocol and the protein content of the extracts were estimated by Lowry's method. Equal amount of protein in Lamillie's buffer was taken and subjected to electrophoresis on 10% SDS-PAGE. The proteins were transferred on to PVDF membrane by Western Blot at 50mA for overnight. The membranes were blocked with 4 % BSA and subsequently washed with PBST (phosphate buffer saline and tween 20). The immunoblot were probed for anti-pERK 1/2 (A) and anti ERK1/2 (B) antibody. The blots were developed using respective horse redox peroxidase (HRP) coupled second antibodies. The colour was developed using West Femto as substrate.  $\beta$ -tubulin was used as internal control. The accompanying graph represents the comparative densitometric/quantitative analysis of the band intensities using image J Launcher (version 1.4.3.67) and arranged in the similar order as of the lanes ERK1 and ERK2 are represented as separate bars. Data are means  $\pm$  SEM of three experiments.

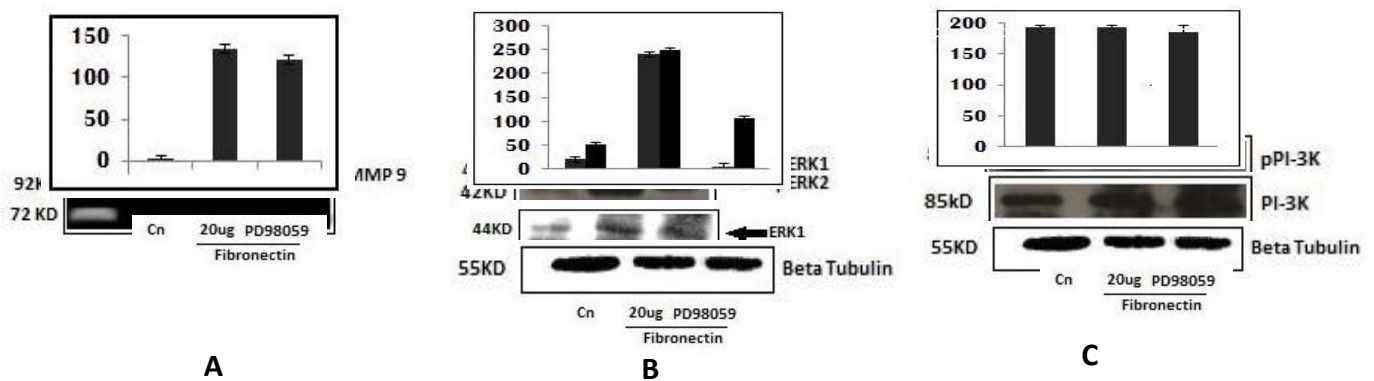


**Figure 3: Effect of ERK Inhibitor 98059**

**A. Comparative zymographic analysis of MMP-9:** Fn (20ug/ml for 16 h) treated and untreated cells were treated with MEK/ERK inhibitor PD98059 (50uM pretreatment for 1 h), and the respective serum free medium was subjected to Gelatin Zymography by standard protocol. The accompanying graph represents the comparative densitometric/quantitative analysis of the band intensities using image J Launcher (version 1.4.3.67) and arranged in the similar order as of the lanes. Data are means  $\pm$  SEM of three experiments.

**B. Effect of MEK/ERK Inhibitor PD98059 on pERK/ERK by Immunoblot:** Fn (20ug/ml for 16 h) treated and untreated B16F10 cells (300,000 cells/ml) were treated with MEK/ERK inhibitor PD98059 (50uM pre-treatment for 1 h), and the respective serum free medium was subjected to Western Blot by standard protocol. The immunoblot were probed for anti-pERK 1/2 and anti ERK1/2 antibody. The blots were developed using respective horse redox peroxidase (HRP) coupled second antibodies. The colour was developed using West Femto as substrate.  $\beta$ -tubulin was used as internal control. The accompanying graph represents the comparative densitometric/quantitative analysis of the band intensities using image J Launcher (version 1.4.3.67) and arranged in the similar order as of the lanes. Data are means  $\pm$  SEM of three experiments.

**C. Effect of MEK/ERK Inhibitor PD98059 on pPI-3K/PI-3K by Immunoblot:** Fibronectin (20ug/ml for 16 hrs) treated and untreated B16F10 cells (300,000 cells/ml) were treated with MEK/ERK inhibitor PD98059 (50 uM pre-treatment for 1 h), and the respective serum free medium was subjected to Western Blot by standard protocol. The immunoblot were probed for anti-pPI3K and anti PI3K antibody. The blots were developed using respective horse redox peroxidase (HRP) coupled second antibodies. The colour was developed using West Femto as substrate.  $\beta$ -tubulin was used as internal control. The accompanying graph represents the comparative densitometric/quantitative analysis of the band intensities using image J Launcher (version 1.4.3.67) and arranged in the similar order as of the lanes. Data are means  $\pm$  SEM of three experiments.

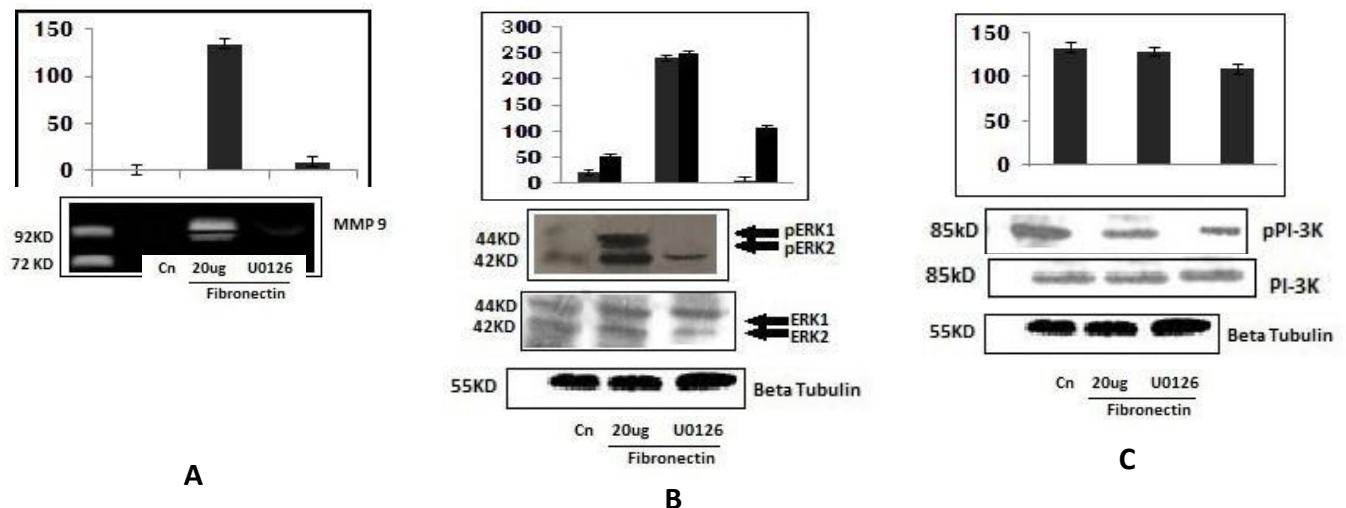


**Figure 4: Effect of MEK/ERK Inhibitor U0126**

**A. Comparative zymographic analysis of MMP9:** Fn (20ug/ml for 16 h) treated and untreated cells were treated with MEK/ERK inhibitor U0126 (25uM pretreatment for 1 h), and the respective serum free medium was subjected to Gelatin Zymography by standard protocol. The accompanying graph represents the comparative densitometric/quantitative analysis of the band intensities using image J Launcher (version 1.4.3.67) and arranged in the similar order as of the lanes. Data are means  $\pm$  SEM of three experiments.

**B. Effect of MEK/ERK Inhibitor U0126 on pERK/ERK by Immunoblot:** Fn (20ug/ml for 16 h) treated and untreated B16F10 cells (300,000 cells/ml) were treated with MEK/ERK inhibitor U0126 (25

uM pre-treatment for 1 h), and the respective serum free medium was subjected to Western Blot by standard protocol. The immunoblot were probed for anti-pERK 1/2 and anti ERK1/2 antibody. The blots were developed using respective HRP coupled second antibodies. The colour was developed using West Femto as substrate.  $\beta$ -tubulin was used as internal control. The accompanying graph represents the comparative densitometric/quantitative analysis of the band intensities using image J Launcher (version 1.4.3.67) and arranged in the similar order as of the lanes. Data are means  $\pm$  SEM of three experiments.

**C. Effect of MEK/ERK Inhibitor U0126 on pPI-3K/PI-3K by Immunoblot:** Fn (20ug/ml for 16 hrs) treated and untreated B16F10 cells (300,000 cells/ml) were treated with MEK/ERK inhibitor U0126 (25uM pre-treatment for 1 h), and the respective serum free medium was subjected to Western Blot by standard protocol. The immunoblot were probed for anti-pPI3K and anti PI3K antibody. The blots were developed using respective HRP coupled second antibodies. The colour was developed using West Femto as substrate.  $\beta$ -tubulin was used as internal control. The accompanying graph represents the comparative densitometric/quantitative analysis of the band intensities using image J Launcher (version 1.4.3.67) and arranged in the similar order as of the lanes. Data are means  $\pm$  SEM of three experiments.

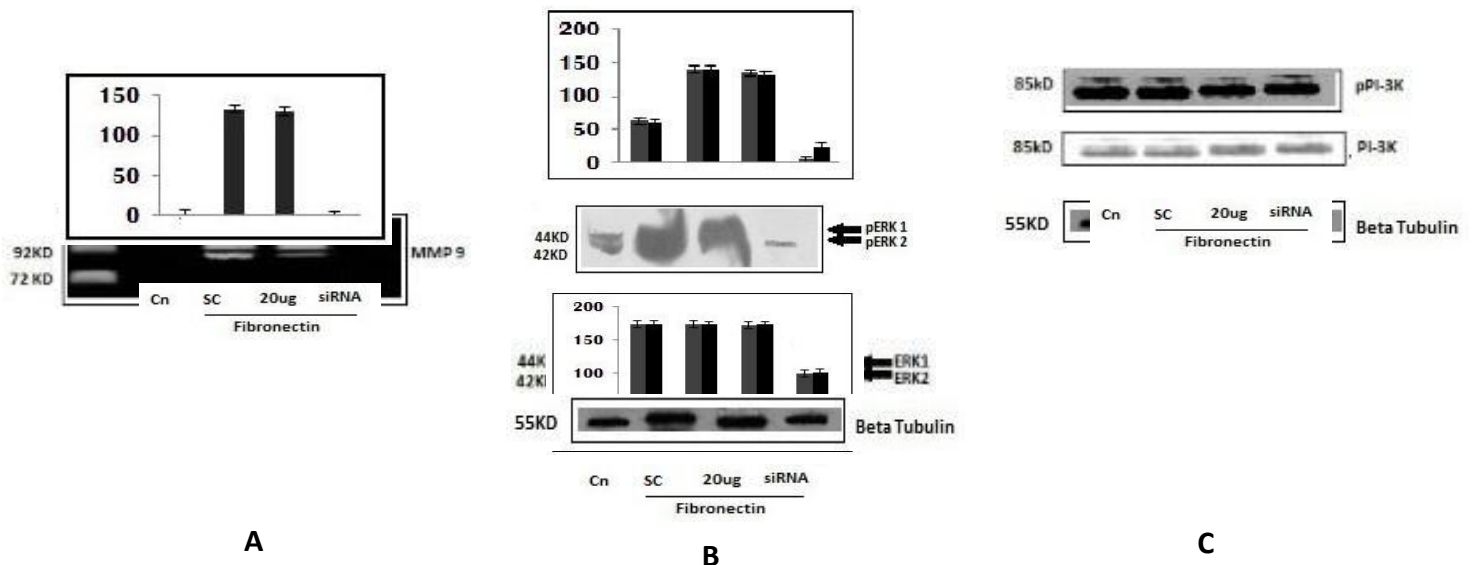


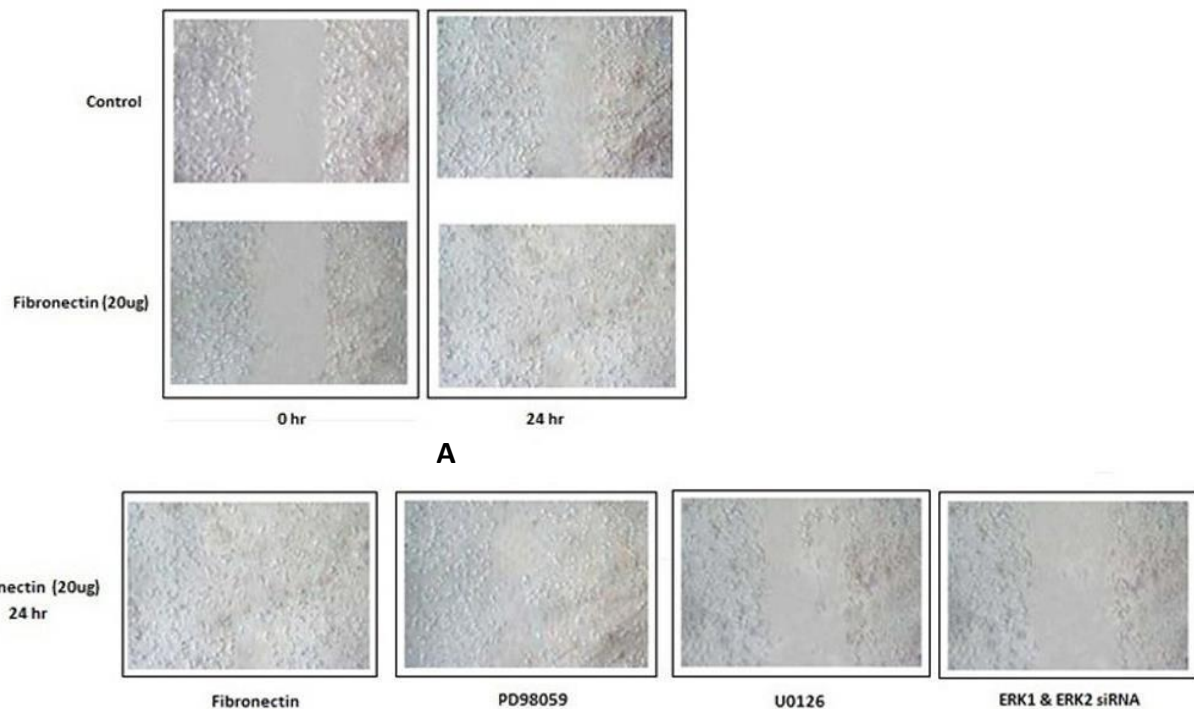
**Figure 5: Effect of double transfection of smart pooled siRNA ERK1 and ERK2**

**A. Comparative zymographic analysis of MMP-9:** Cells were seeded in 35 mm dishes and grown to 60% confluence. For the transfection process, ERK1 siRNA, ERK 2 siRNA and negative control siRNA were transfected using Lipofectamine<sup>TM</sup> 2000 following standard protocol of sequential double transfection. Cells were then treated with Fibronectin (20ug/ml for 16 h) and the respective serum free medium was subjected to Gelatin Zymography by standard protocol. The accompanying graph represents the comparative densitometric/quantitative analysis of the band intensities using image J Launcher (version 1.4.3.67) and arranged in the similar order as of the lanes. Data are means  $\pm$  SEM of three experiments.

**B. Effect of ERK1 and ERK2 siRNA on pERK/ERK by Immunoblot:** Cells were seeded in 35 mm dishes and grown to 60% confluence. For the transfection process, ERK1 siRNA, ERK 2 siRNA and negative control siRNA were transfected using Lipofectamine<sup>TM</sup> 2000 following standard protocol of sequential double transfection. Cells were then treated with Fibronectin (20ug/ml for 16 h) and the respective serum free medium was subjected to Western Blot by standard protocol. The immunoblot were

probed for anti-pERK 1/2 and anti ERK1/2 antibody. The blots were developed using respective horse redox peroxidase (HRP) coupled second antibodies. The colour was developed using West Femto as substrate.  $\beta$ -tubulin was used as loading control. The accompanying graph represents the comparative densitometric/quantitative analysis of the band intensities using image J Launcher (version 1.4.3.67) and arranged in the similar order as of the lanes. Data are means  $\pm$  SEM of three experiments.

**C. Effect of ERK1 and ERK2 siRNA on PI-3K/pPI-3K by Immunoblot:** Cells were seeded in 35 mm dishes and grown to 60% confluence. For the transfection process, ERK1 siRNA, ERK 2 siRNA and negative control siRNA were transfected using Lipofectamine™ 2000 following standard protocol of sequential double transfection. Cells were then treated with Fibronectin (20ug/ml for 16 h) and the respective serum free medium was subjected to Western Blot by standard protocol. The immunoblot were probed for anti-PI-3K and anti PI-3K antibody. The blots were developed using respective HRP coupled second antibodies. The colour was developed using West Femto as substrate.  $\beta$ -tubulin was used as loading control. The accompanying graph represents the comparative densitometric/quantitative analysis of the band intensities using image J Launcher (version 1.4.3.67) and arranged in the similar order as of the lanes. Data are means  $\pm$  SEM of three experiments.



**A.** B16F10 cells (300,000 cells/ml) were grown in serum free culture medium in absence (control) and in presence of Fn (20ug/ml) for 16 h. The monolayer was scratched with a sterile pipette tip, followed by washing thrice with SFCM to remove cellular debris. The cells were maintained in fresh SFCM and cell migration was observed by microscopy and documented by photography at 0 hr and 24 h.

**B.** ERK/MEK Inhibitor PD98059, U0126, ERK1 /2 siRNA or Control SiRNA treated cells were cultured in a monolayer in absence and presence of fibronectin (20 mg/ml) for 16 h. The monolayer was scratched with a sterile pipette tip, followed by washing thrice with SFCM to remove cellular debris. The cells were maintained in fresh SFCM and cell migration was observed by microscopy and documented by digital photography at 0 h and 24 h.

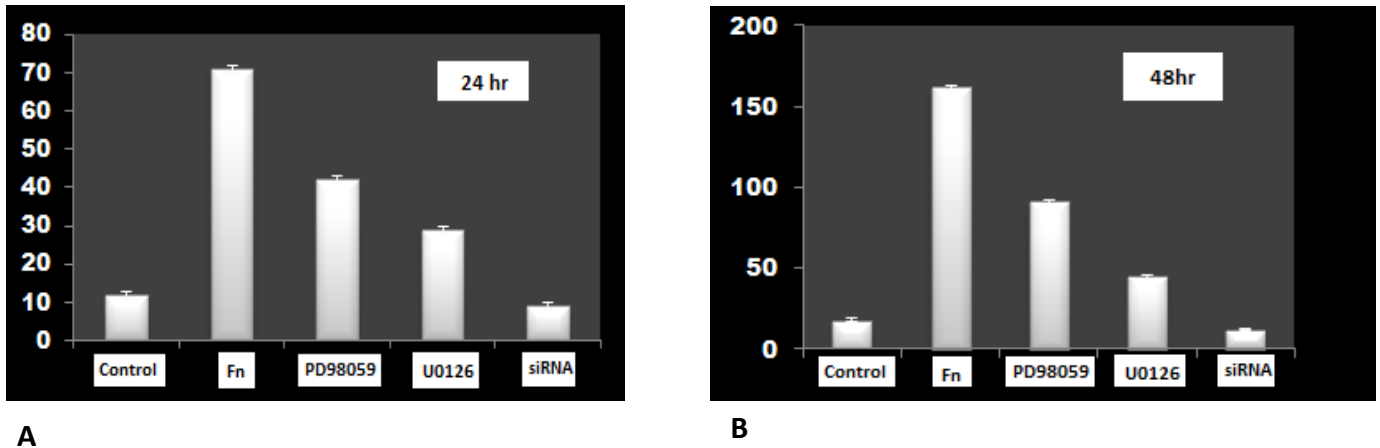


**Figure 7: Effect of Inhibition of ERK1 /2 on Cell invasion**

ERK/MEK Inhibitor PD98059, U0126, ERK1 /2 siRNA or Control SiRNA treated cells were cultured in transwell chambers in triplicate in absence and presence of fibronectin (20 mg/ml) for 16 h. The chamber was inserted in DMEM containing 5% FBS as chemo-attractant and grown for 24 h (A) and 48 h (B). The chambers were then removed, washed. The cells migrated on the membrane were observed under microscope. Number of B16F10 cells migrated through transwell insert were counted per microscopic power field.

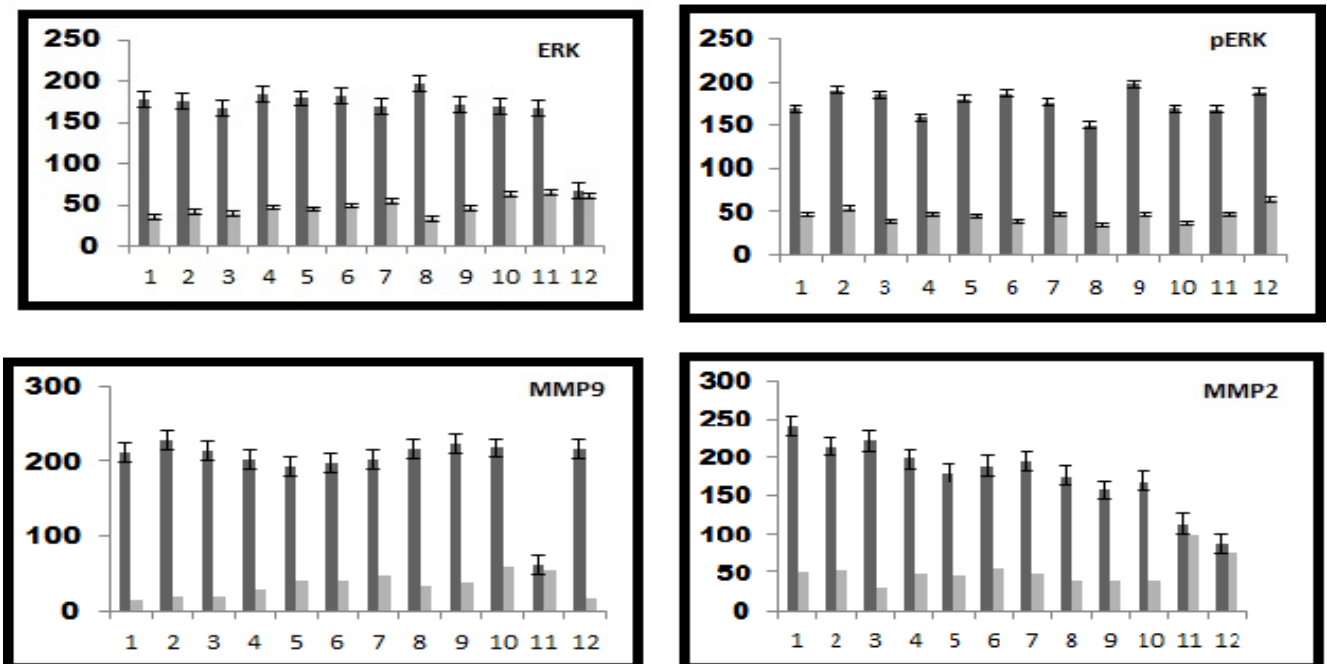


**Figure 8: Co-relation between ERK, ERK, MMP 9 and MMP 2 in mice tumor in control and contralateral tissue.**

Parameters	HIGH	p values
ERK	11	0.011
pERK	12	0.002
MMP9	12	0.002
MMP2	11	0.011

**Table 1. Statistical parameters of ERK, pERK, MMP 9 and MMP 2 in mice tumor in control and contralateral tissue**

B16F10 cell suspensions ( $5 \times 10^5$  cells in 0.1 ml PBS) were injected subcutaneously into the right flank of each mouse at the concentration of  $1 \times 10^6$  cells per Black syngeneic C57BL/6J mouse. Following implantation in 12 mice, tumors were monitored daily for palpable tumor masses, and tumor length and width were observed. The tumor endpoint of 4.0 to 5.0 /per  $\text{cm}^3$  was adopted for tumor size. Mice were sacrificed via CO<sub>2</sub> asphyxiation in accordance with IACUC guidelines. Tumors were excised and protein was harvested from both tumor tissues and contralateral (normal) tibia following standard protocol. Equal amount of protein was charged for Western Blot and probed for ERK, pERK. Similarly, gelatin zymography was performed from equal amount of tumor samples. The accompanying graph represents the comparative densitometric/quantitative analysis of the band intensities of Control and Contralateral (Normal) tissue using image J Launcher (version 1.4.3.67).

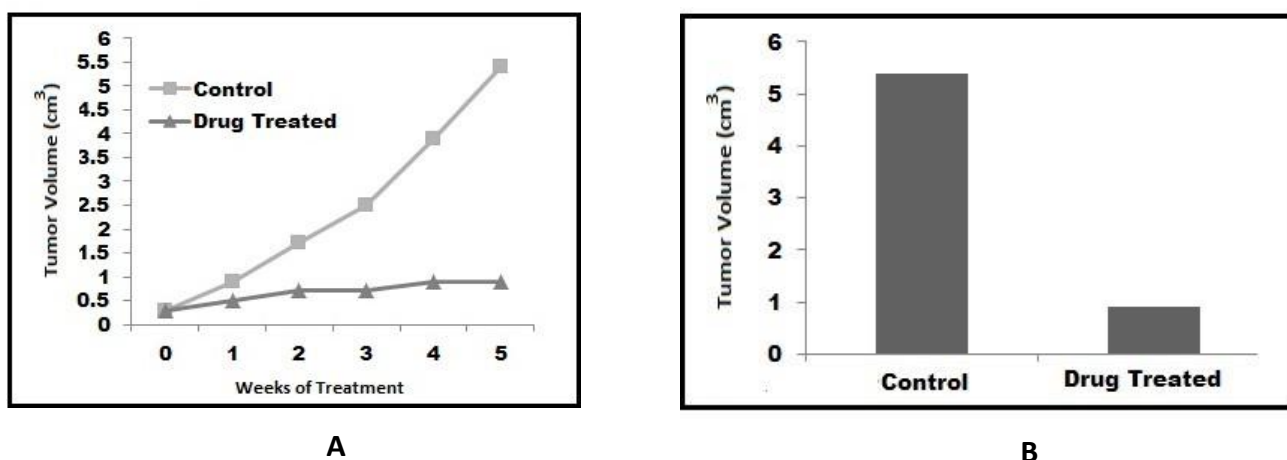


**Figure 9: Effect of ERK/MEK inhibitor U0126 on mice xenograft.**

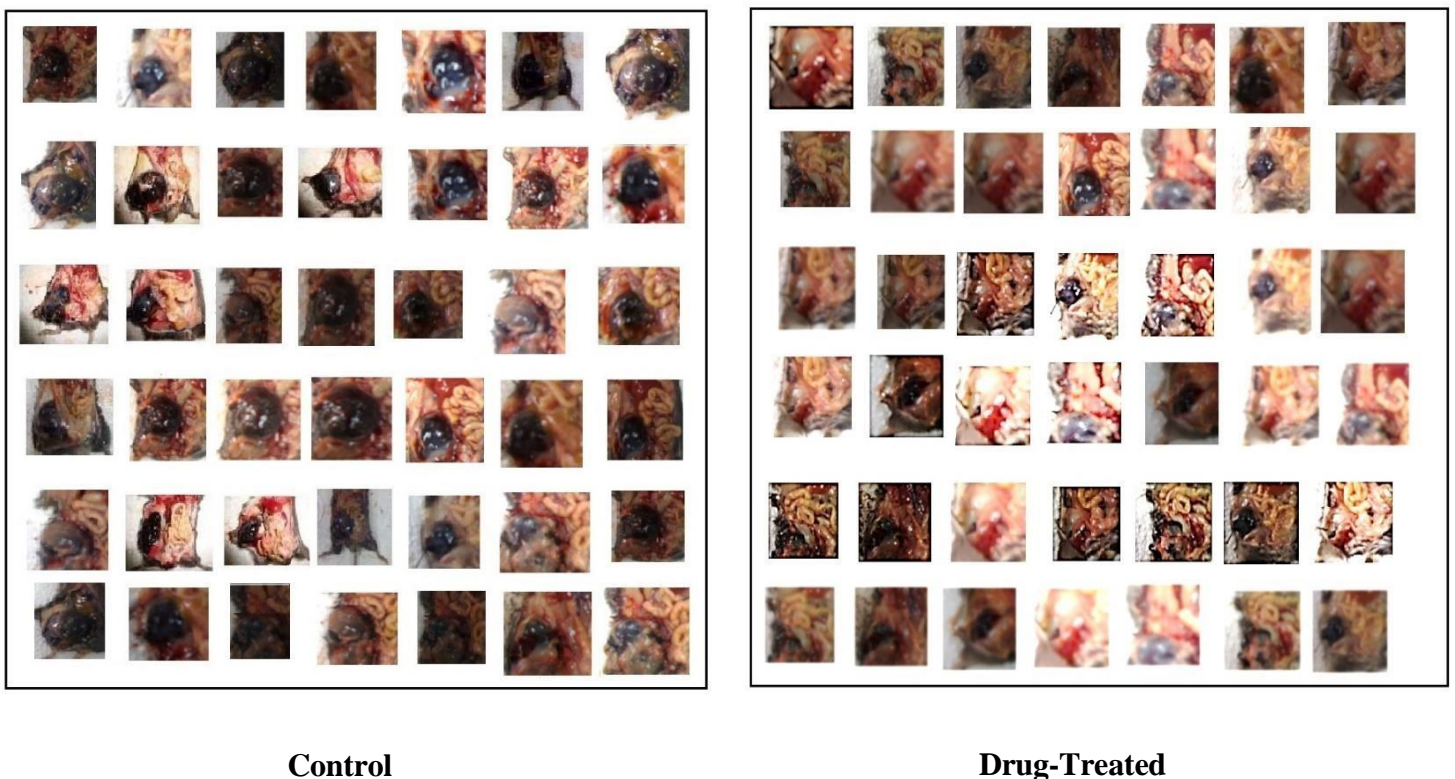
Experimental Sets	Tumour Size (in $\text{cm}^3$ )						Total
	<1		3		>5		
	Number	%	Number	%	Number	%	
Control	2	4.76	0	0.00	40	95.24	42
Drug treated	39	92.86	1	0.02	2	4.76	42

**Table 2: Distribution of tumor size in control and drug treated sets**

B16F10 cell suspensions ( $5 \times 10^5$  cells in 0.1 ml PBS) were injected subcutaneously into the right flank of each mouse at the concentration of  $1 \times 10^6$  cells per Black syngeneic C57BL/6J mouse. Following implantation in mice, tumors were monitored daily for palpable tumor masses, and tumor length and width were observed. Tumor size was measured by calliper according to the following formula:  $\text{volume} = (\text{width})^2 \times \text{length} / 2$ . The tumor endpoint of 4.0 to 5.0 /per  $\text{cm}^3$  was adopted for tumor size. After tumor size reached  $0.3\text{cm}^3$  the mice were divided in 2 groups, 42 each. U0126 treatment (25  $\mu\text{mol/kg}$ ) through I.P injections was started in one group whereas the control group received 200  $\mu\text{l}$  carrier solutions. Treatments were administered weekly for 5 weeks. Mice were sacrificed via CO<sub>2</sub> asphyxiation in accordance with IACUC guidelines.

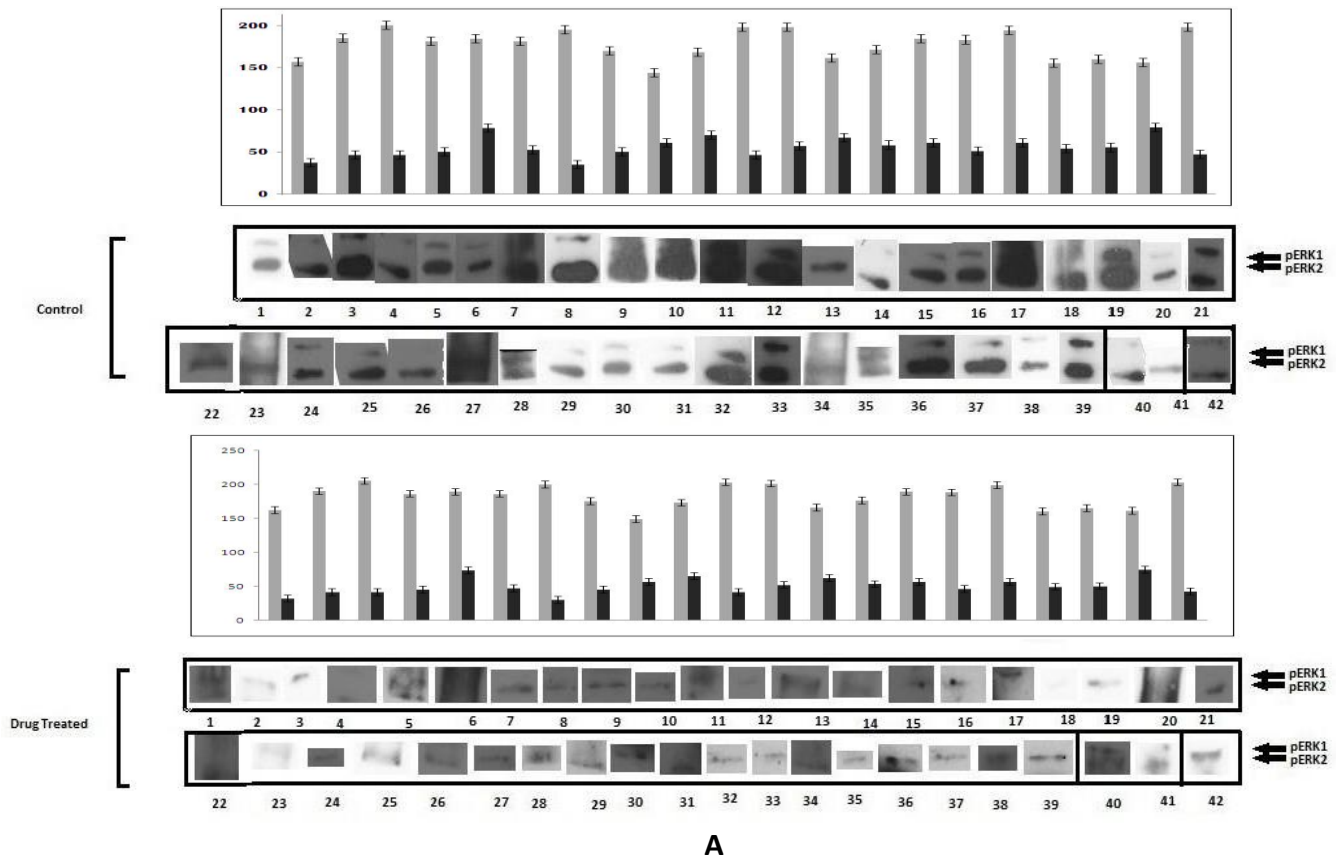
**A.** Comparative growth curves of Tumor sizes (mean +/- SD) between Control and Drug-treated mice groups throughout 5 weeks.

**B.** Comparison of average tumor size (mean+/-SD) between Control and Drug-treated mice groups in excised tumors.



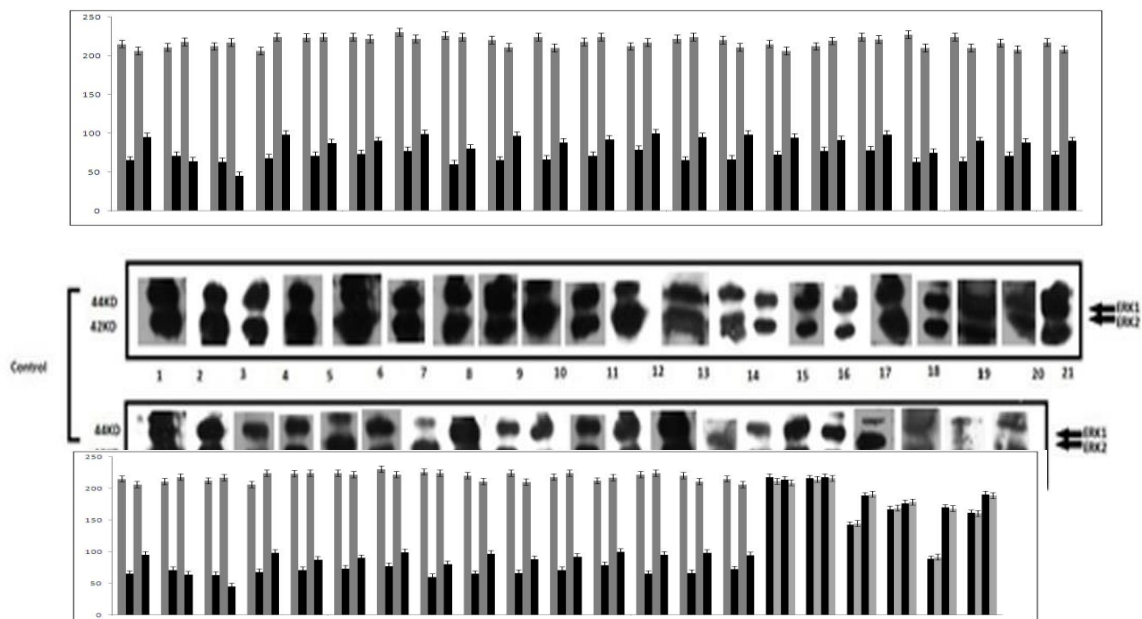
**Figure 10: Representative images of mice tumors in Control and drug treated groups**

B16F10 cell suspensions ( $5 \times 10^5$  cells in 0.1 ml PBS) were injected subcutaneously into the right flank of each mouse at the concentration of  $1 \times 10^6$  cells per Black syngeneic C57BL/6J mouse. Following implantation in mice, tumors were monitored daily for palpable tumor masses, and tumor length and width were observed. Tumor size was measured by caliper according to the following formula:  $\text{volume} = (\text{width})^2 \times \text{length} / 2$ . The tumor endpoint of 4.0 to 5.0 /per  $\text{cm}^3$  was adopted for tumor size. After tumor size reached  $0.3\text{cm}^3$  the mice were divided in 2 groups, 42 each. U0126 treatment (25  $\mu\text{mol/kg}$ ) through I.P injections was started in one group whereas the control group received 200  $\mu\text{l}$  carrier solutions. Treatments were administered weekly for 5 weeks. Mice were sacrificed via CO<sub>2</sub> asphyxiation in accordance with IACUC guidelines. Mice were dissected and tumors captured through digital photography.



**Figure 11 A: Effect of MEK/ERK Inhibitor on activity of pERK in Mouse xenografts**

Proteins from Mouse xenografts, Control and Drug-treated were harvested and equal amount of protein was loaded for Western Blot. The Blots was probed for pERK. Lanes in between are spliced off.  $\beta$ - tubulin (not shown) was used as loading control. The accompanying graph represents the comparative densitometric/quantitative analysis of the band intensities using image J Launcher (version 1.4.3.67) and are arranged in accordance with the lanes.



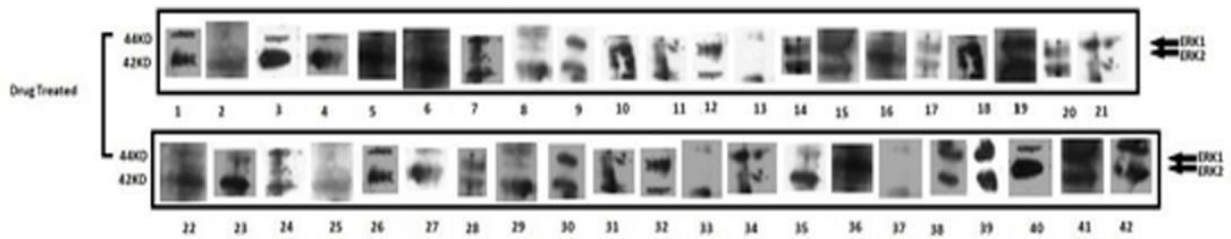


**Figure 11 B: Effect of MEK/ERK Inhibitor on activity of ERK in Mouse xenografts**

Proteins from Mouse xenografts, Control and Drug-treated were harvested and equal amount of protein was loaded for Western Blot. The Blots was probed for ERK. Lanes in between are spliced off.  $\beta$ -tubulin (not shown) was used as loading control. The accompanying graph represents the comparative densitometric/quantitative analysis of the band intensities using image J Launcher (version 1.4.3.67) and are arranged in accordance with the lanes.

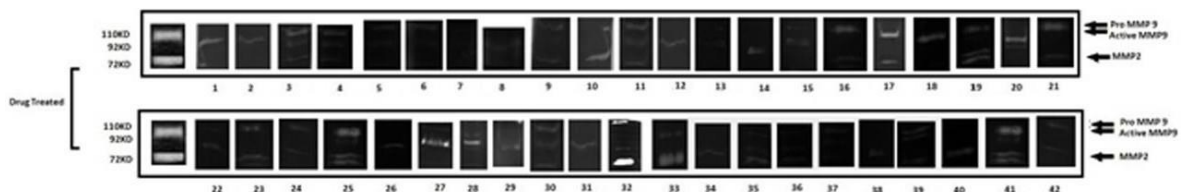
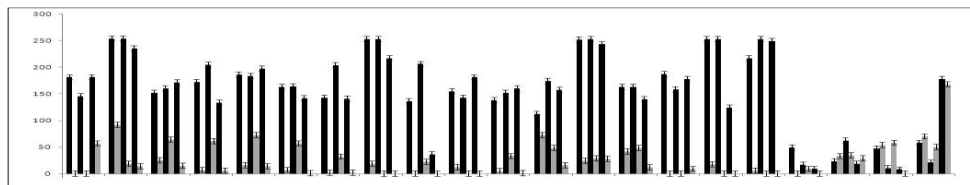
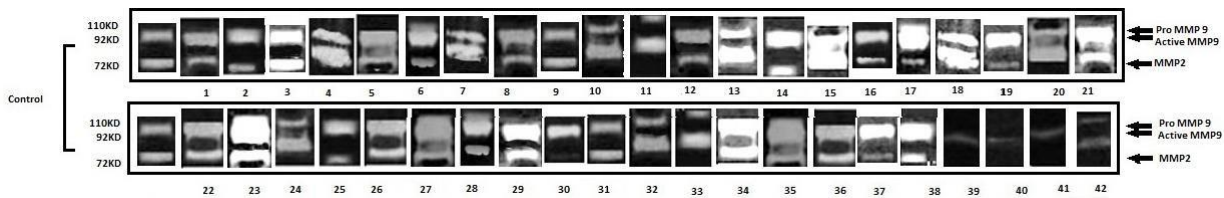
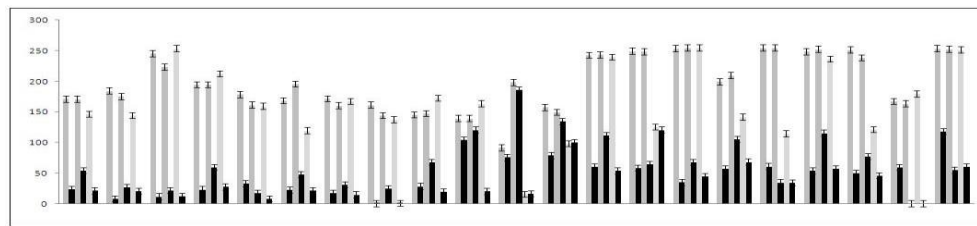


**Figure 12 A: Effect of MEK/ERK Inhibitor on activity of MMP9/MMP2 in Mouse xenografts**

Proteins from Mouse xenografts, Control and Drug-treated were harvested and equal amount of protein was loaded for Gelatin Zymography for detection of MMP9 and/or MMP2 activity. Lanes in between are spliced off. The accompanying graph represents the comparative densitometric/quantitative analysis of the band intensities using image J Launcher (version 1.4.3.67) and are arranged in accordance with the lanes.

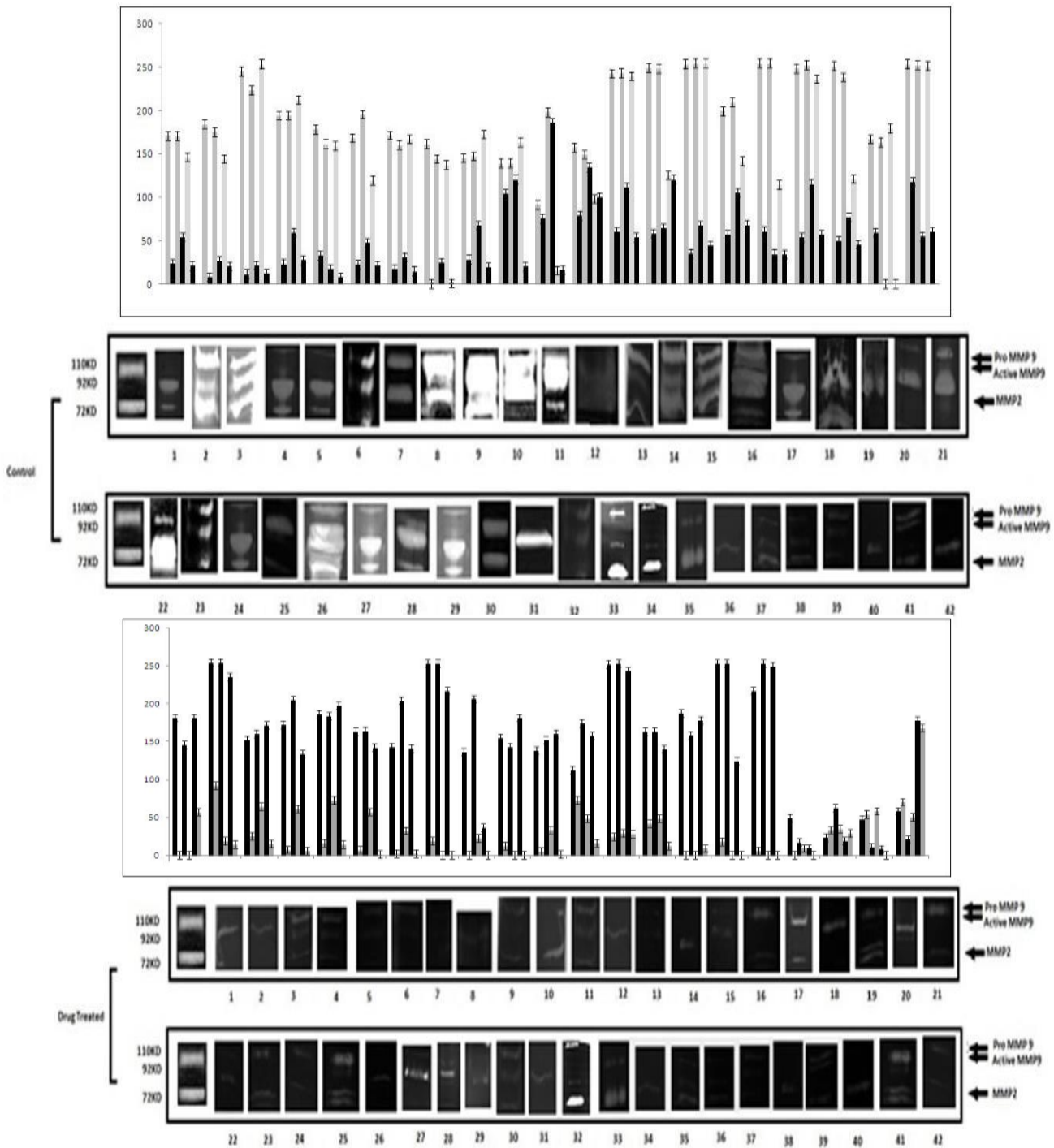


**Figure 12 B: Effect of MEK/ERK Inhibitor on activity of MMP9/MMP2 in Mouse serum** Fresh blood was collected from sacrificed mice of both the groups and serum was isolated following standard protocol. Control and Drug-treated were harvested and equal amount of protein was loaded for Gelatin Zymography for detection of MMP9 and/or MMP2 activity. Lanes in between are spliced off. The accompanying graph represents the comparative densitometric/quantitative analysis of the band intensities using image J Launcher (version 1.4.3.67) and are arranged in accordance with the lanes.



**Figure 13: Co-relation between ERK and pERK with pRKIP/RKIP/TIMP1/TIMP2 in Mouse xenografts**

Proteins from Mouse xenografts, Control and Drug-treated were harvested and equal amount of protein was loaded for Western Blot. The Blots was probed for pRKIP, RKIP, TIMP1 and TIMP2. Lanes in between are spliced off.  $\beta$ -tubulin (not shown) was used as loading control.

Parameters	High	Similar	Low	p values
ERK	37	5	-	0.001
pERK	39	2	1	0.0001
MMP9	38	3	1	0.001
MMP2	35	7	-	0.01
MMP9 (Blood Serum)	31	11	-	0.01
MMP2 (Blood Serum)	31	11	-	0.01
TIMP 1	6	3	33	0.01
TIMP 2	5	4	33	0.01
RKIP	-	-	42	0.000001

**Table 3: values of parameters with control group with respect to treated group**

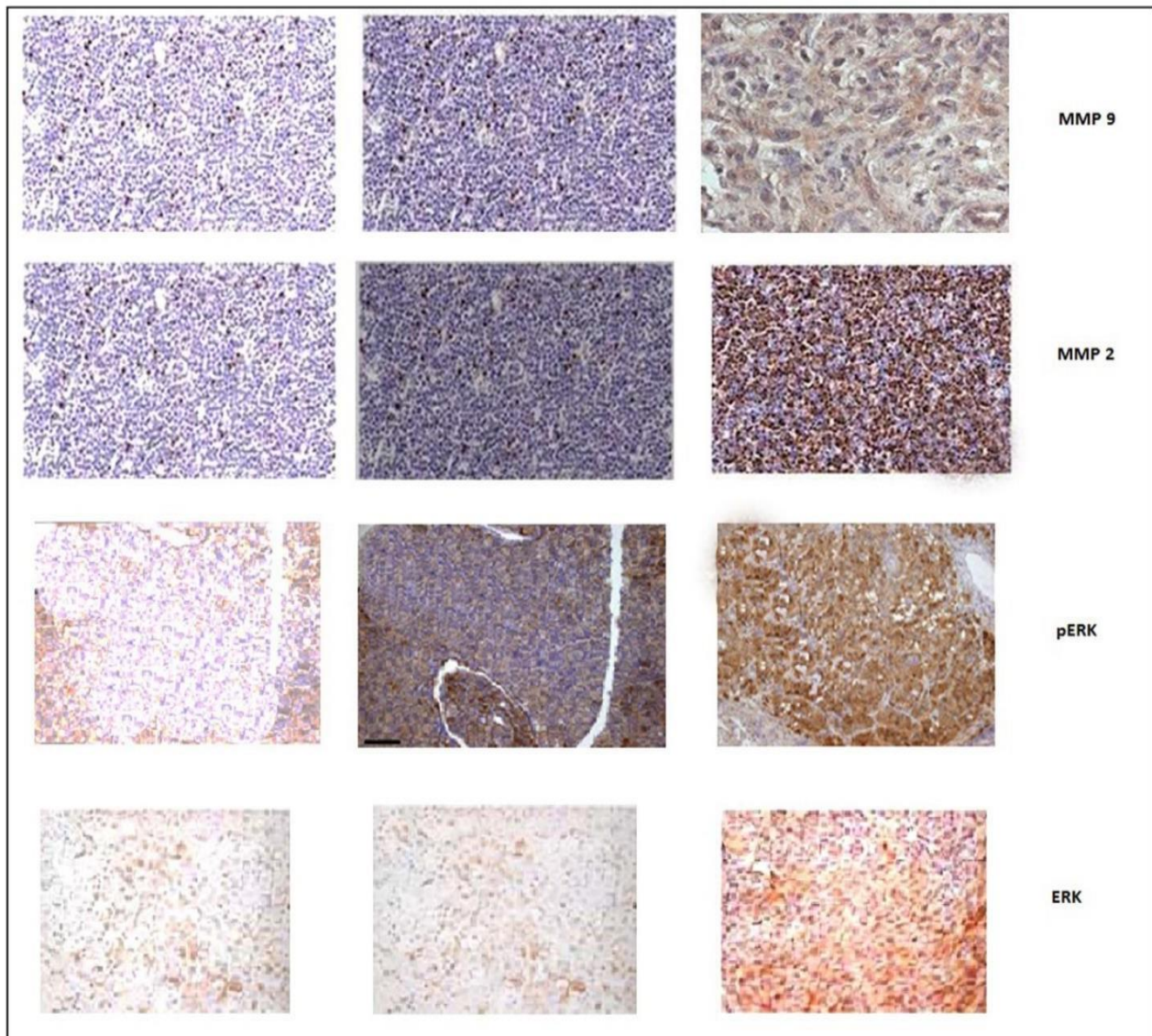


**Figure 14: Representative images showing expression of MMP 2, MMP9, ERK and pERK by immunohistochemistry of excised tumor cross-sections.**

Control and Drug (U0126) treated samples were fixed in 10% neutral buffered formalin processed routinely and embedded in paraffin. The sections were de-paraffinized in xylene, re-hydrated in Et-OH, and washed twice with distilled water. For better antigen retrieval, the samples were boiled three times for 5 minutes in a microwave in citrate buffer (10mM, pH-6). Endogenous per-oxidases were blocked by 5% hydrogen peroxidase treatment for 5 mins. The samples were washed with PBS (pH-7.2) and incubated in 2% normal bovine serum for 35 mins to prevent nonspecific antigen binding followed by incubation with the primary antibody for ERK, pERK, MMP-9 (C-20) and MMP2, at a working dilution of 1:500 for overnight at 4°C. Before applying the secondary antibody, the samples were washed twice with PBS. The slides were then incubated with the biotinylated secondary antibody followed by a wash and a 50 minutes incubation in avidin-biotinylated peroxidase complex reagent. Expressions were visualized with a 5 mins diaminobenzidin tetrahydrochloride treatment. The slides were counterstained with Mayer's hematoxylin, dehydrated and mounted with DPX. A routinely processed tumor section without the primary antibody served as negative control at each staining series. Data are means  $\pm$  SEM of three experiments.

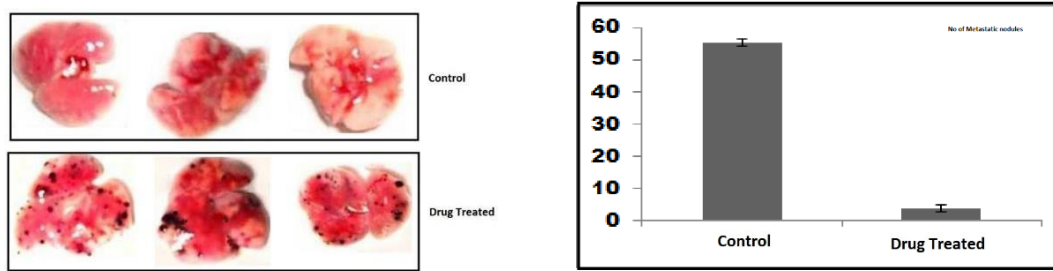


**Figure 15: Evaluation of Lung metastasis in Control and Drug treated mice**

Lungs were isolated from mice after dissection. Figure shows representative examples of lungs and quantitative evaluation of macroscopically detectable lung metastases. Accompanying graph represents the average number of Metastatic lung nodule present in Control and Drug treated mice. Data are means  $\pm$  SEM of 42 mice.

Experimental Sets	Tumour Size (in cm <sup>3</sup> ) (n=42)					
	<1		3		>5	
	No. of lung metastasis	%	No. of lung metastasis	%	No. of lung metastasis	%
Control	0	0.00	0	0.00	36	85.17
Drug treated	4	9.52	0	0.00	2	4.76

**Table 4: Distribution of lung metastasis with respect to tumor size**

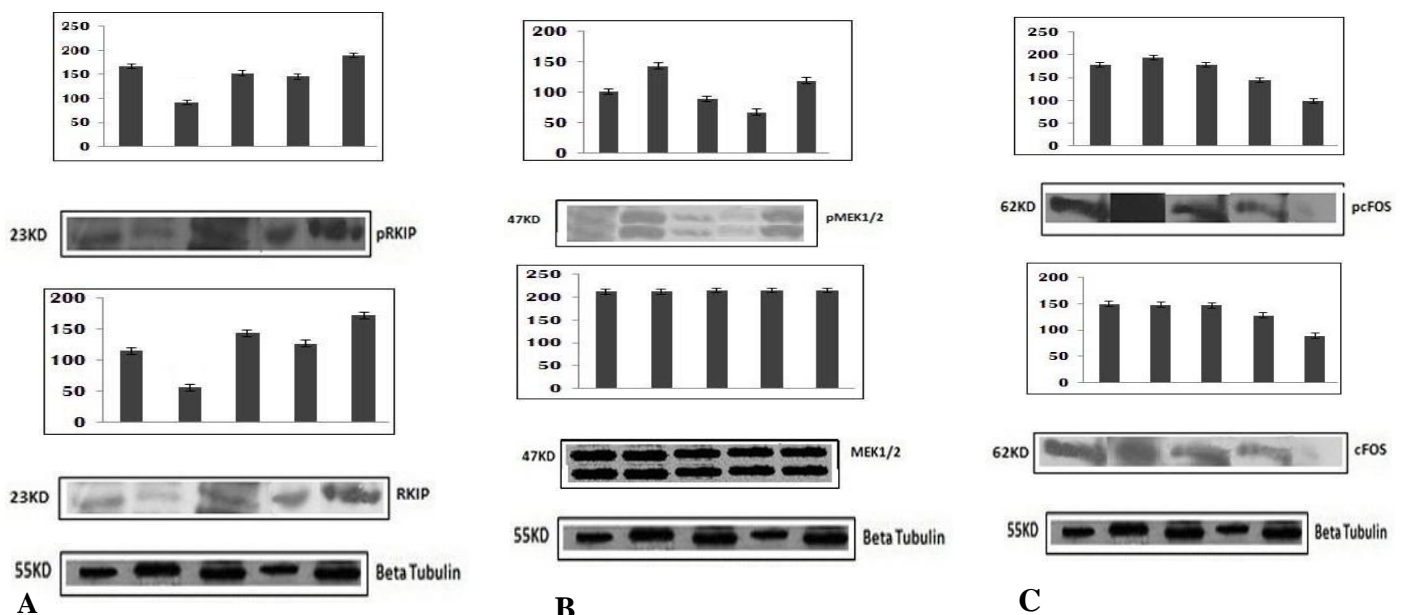


**Figure 16: Effect of modulation of ERK on upstream and downstream molecules**

ERK/MEK Inhibitor PD98059, U0126, ERK1 /2 siRNA or Control SiRNA treated cells were cultured in a monolayer in absence and presence of fibronectin (20 mg/ml) for 16 h. The cells were then harvested and the equal amount of protein was subjected to immunoblot. The blot was probed for (A) pRKIP and RKIP, (B) pMEK1/2 and MEK1/2, (C) pcFOS and cFOS. Beta tubulin was used as internal control. The accompanying graph represents the comparative densitometric/quantitative analysis of the band intensities using image J Launcher (version 1.4.3.67) and are arranged in accordance with the lanes.

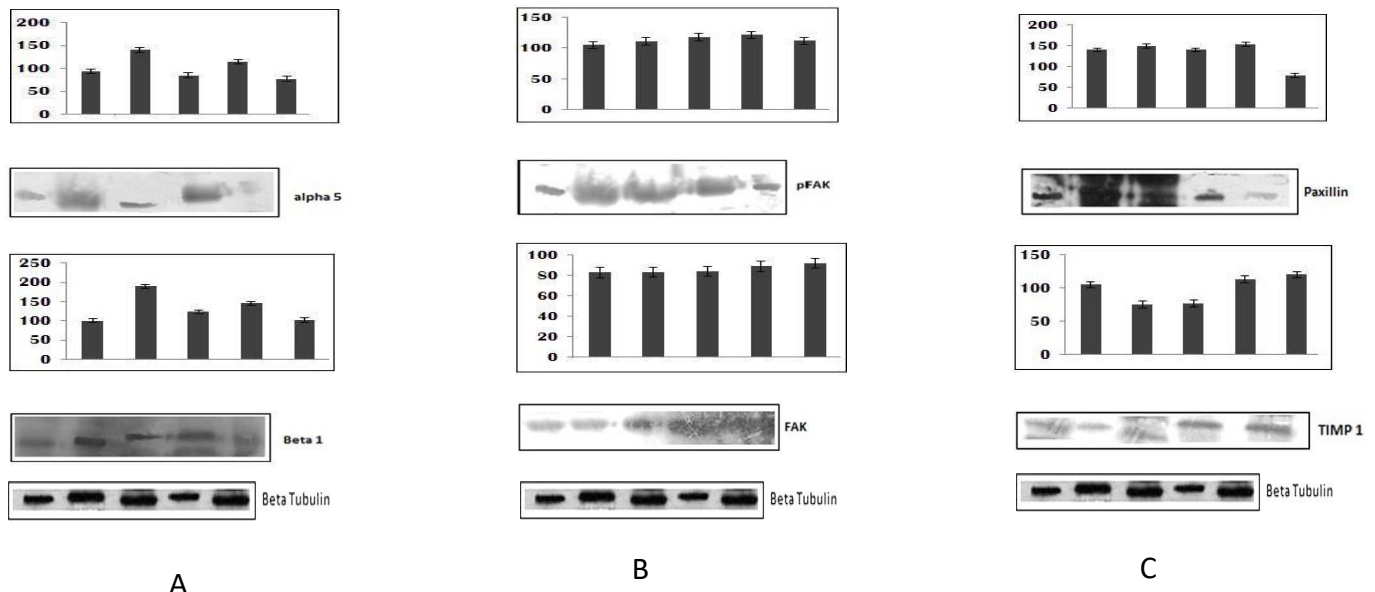


**Figure 17: Effect of modulation of ERK on integrin and cell adhesion molecules**

ERK/MEK Inhibitor PD98059, U0126, ERK1 /2 siRNA or Control SiRNA treated cells were cultured in a monolayer in absence and presence of Fn (20 mg/ml) for 16 h. The cells were then harvested and the equal amount of protein was subjected to immunoblot. The blot was probed for (A)  $\alpha$  5 and  $\beta$  1, (B) pFAK and FAK, (C) paxillin and TIMP1.  $\beta$  tubulin was used as internal control. The accompanying graph represents the comparative densitometric/quantitative analysis of the band intensities using image J Launcher (version 1.4.3.67) and are arranged in accordance with the lanes.

MMPs are the family of endopeptidases that are both structurally and functionally related, dependent on zinc for its activity and degrades extracellular matrix components like fibronectin, membrane collagens and proteoglycans. MMPs play a major role in tumor cell invasiveness and metastasis (Malemud, 2006). MMP 9 can be used as a target in developing anti-cancer therapies as its role is pivotal in tumor cell invasiveness and metastasis. Tumor cells on interaction with Fn is able to facilitate the expression of MMP-9 and hence promoting cell migration and cell invasive property triggering a downstream cascade of cell signaling regulated by integrin receptors. Expression of MMP-9 is much more in the malignant cells than in the non-invasive and benign tumor cells. Figure 1A zymogram shows a Fn dose dependent activation of both the pro-active and active bands of MMP-9. Similar results were found by (Das et al., 2008) who concluded quick activation and expression of MMP-2 and MMP-9 when human breast carcinoma cells were exposed to Fn. Also, (Sen et al., 2010) reported similar result in human laryngeal cancer cells where there was Fn induced increase in MMP-9 expression on binding with  $\alpha$  5  $\beta$  1 integrin receptors through FAK, PI-3K/ERK and ILK signaling pathways. The Image J analysis shows a 4-fold

increase of the cells treated with 20 ug Fn. The expression of the same cells didn't change when observed through western blot as shown in Figure 1B.

Fn is an interesting matrix component in cancer and in mouse models decreased circulation of Fn leads to decreased size of tumors. Absence of Fn leads to decreased cancer progression. This decrease in carcinogenic cell proliferation might lead to decrease in the phosphorylation of ERK. Hence modulating matrix can be an adjuvant to traditional cancer therapies as long as we obtain depletion in Fn (Hackl et al., 2021). But there are evidences where Fn helps in cell proliferation by stimulating the phosphorylation of ERK. This ultimately is translocated to the nucleus causing reduction in apoptotic signals and helping in progression of the cell cycle (Ebner et al., 2007). FN binds with  $\alpha 5 \beta 1$  integrin leading to ERK activation (Cao et al., 2015; Kohno and Pouyssegur, 2009; Shin et al., 2020). In our study we obtained similar results as there was a dose dependent increase in the activity of pERK 1/2 with increasing concentration of Fn as shown in Figure 2 A. In figure 2B, the expression of ERK 1/2 remained similar all through as seen. The expression of the same cells didn't change when observed in western blot. All the immunoblots were subjected to internal controls and no change was observed.

Figure 3A shows the effect of ERK/MEK inhibitor PD98059 on the activity of MMP9 by Zymography. The zymogram shows a small decrease in the intensity of MMP 9 band in the inhibitor treated cells with respect to Fn treated cells. There was marked decrease in the intensity of the pERK1/2 (Figure 3 B), though the total ERK1/2 remains unchanged. The expression and activity of PI-3K (Figure 3 C) was also checked by western blot and negligible variation was observed. Our previous work reported the inhibitory effect of MEK/ERK inhibitor PD98059 on ERK 1/ 2 MMP9 and MMP2 (Moulik et al., 2014) in human breast cancer cell lines MCF-7 and MDA-MB-231. No inhibitory effect of PD98059 was found in the protein content of both MMP9 and MMP2 in both MCF-7 and MDA-MB-231. It was also found out that the dephospho ERK 1/ 2 remained unaltered by the inhibitor treatment (Moulik et al., 2014) .

Inhibition of MEK/ERK affects the angiogenic signaling pathway and growth in tumor cells. There lies a strong correlation between inhibition of MEK/ERK and tumor growth arrest (Mayes et al., 2013; Merchant et al., 2017). Cancer immunotherapies based on signal transduction can make good use of MEK inhibitors (Marampon et al., 2009). In our study there was an appreciable decrease in the MMP9 activity when Fn treated B16F10 cells were treated with U0126 (Figure 4A). The activity of pERK1/2 also corresponded likewise as shown in Figure 4B, though the levels of total ERK1/2 and pPI-3k level remained unaltered. A small change in the pPI-3K levels was observed (Figure 4 C).

Invasiveness of tumor cells is inhibited when different MMPs are downregulated by blockage of ERK pathway double transfection of ERK1-siRNA and ERK2-siRNA strengthens the fact that ERK inhibits MMP2 and MMP9 activities (Invasiveness and Cell, 2014; Tanimura et al., 2003) .Figure 5 A showed a marked inhibitory effect of ERK1/2 and siRNA on the activity of MMP9 almost beyond detection limit in Fn treated B16F10 cells. Activity of ERK was also largely diminished by siRNA which corresponded in both dephospho and phospho protein levels. PI-3K levels were checked as an indicator of siRNA effect on parallel signaling pathways (Bessard et al., 2008; He et al., 2014) and no effect was detectable by immunoblots. The results of our study are in accordance with our previous report on human cancer cell lines MCF-7 and MDA-MB-231 (Moulik et al., 2014) .The study reported 80% decrease in the levels of phosphorylation of ERK1/2 and also the same in the dephospho levels in the MCF-7 cell line. siRNA treatment further led to sharp declination in MMP2 and MMP9 levels. It suggested a correlation among ERK, MMP2 and MMP9 in both the human cancer cell lines.

ERK is an important regulator of cell motility. Hence signaling pathway of ERK is regarded as a promising

therapy for cancer (Caunt et al., 2015; Sengupta et al., 2022; Tanimura and Takeda, 2017). Invasion occurs when cells migrate along the extracellular matrix, vessels and neurons in canonical mesenchymal fashion. Malignant cells migrate as sheets maintaining adhesion among the cells where leader cells present at the edge of the sheet directs efficient movement of the cells by cell protrusion (Paul et al., 2016; Reffay et al., 2014; Samson et al., 2022). Cell proliferation, cancer-stromal interaction and metastasis is significantly decreased due to the action of ERK inhibitors and process of autophagy. Metastatic nodules are largely reduced by ERK inhibitor treatment (Yan et al., 2019). In our study, the rate of cell migration of B16F10 cells was checked by Cell migration assay (Figure 6). There was an appreciable decrease in the growth rate of U0126 treated B16F10 cells with respect to PD9059 treated cells. The rate of cell migration reduced markedly when cells were treated with ERK1/2 siRNA. The pattern of marked and gradual decrease in the rate of cell migration with the treatment of PD98059, U0126 and siRNA 1/2 were found to be similar also in cell invasion assay where cells were subjected to aforesaid treatments and cultured over a period of 48hrs in trans well chambers.

The pattern of marked and gradual decrease in the rate of cell migration with the treatment of PD98059, U0126 and siRNA 1/2 were found to be similar also in cell invasion assay where cells were subjected to aforesaid treatments and cultured over a period of 48hrs in trans well chambers. Figure 7 (A and B) shows the number of B16F10 cells migrated through trans well insert which were counted per microscopic power field. Similar findings were stated by (Yan et al., 2019) in splenic pancreatic cancer organoid xenograft mouse in mouse model.

Table 1 shows Paired-sample Wilcoxon signed-rank test. The test was used to compare the values of ERK/ pERK with MMP2/MMP9 between control and contralateral sets of tumor samples from B16F10 injected mice. All the statistical tests were performed with the help of SPSS (version – 20).  $p < 0.05$  was taken to be statistically significant. All the values of Control were compared with Contra lateral and were designated as HIGH or LOW as per Image J analysis (Figure 8). In control ERK, 11 values out of 12 values were higher with respect to Contra lateral and only 1 value was similar. Now Paired-sample Wilcoxon signed-rank test showed that the values of Control ERK were significantly higher ( $p = 0.011$ ). Also, in pERK all the 12 values of control were higher than the contra lateral. Test also showed that the values of control pERK were significantly higher ( $p = 0.011$ ) in all the 12 cases. The values of MMP9 were high in all 12 samples compared to contra lateral which was significant ( $p = 0.002$ ). The values of control MMP2 were high in 11 samples out of 12 with respect to contra lateral ( $p = 0.002$ ). The significant increase in activity of pERK/ERK along with MMP9 and MMP2 may carry an interrelation between them.

Figure 9 (A and B) shows the effect of ERK/MEK inhibitor U0126 on mice xenografts where the gradual increase of the tumor volume in the Control mice is appreciable higher than Drug treated mice. The comparison of average tumor volume also confirms the increase. Table 2 represents the distribution of tumor size. Test of proportion showed that proportion of tumor size  $< 1 \text{ cm}^3$  was significantly lower in control group compared to drug treated group ( $p = 0.00001$ ). No significant difference was found for tumor size  $= 3 \text{ cm}^3$  in the two groups ( $p = 0.62$ ). Also, the proportion of tumor size  $> 5 \text{ cm}^3$  was significantly lower in drug treated group ( $p = 0.000001$ ). Thus, the drug had significantly reduced the tumor size. (Marampon et al., 2009) also reported 48% reduced tumor growth, reduced phospho-active ERK and c-Myc expression in rhabdomyosarcoma cells treated with U0126. Our previous report showed a sharp decrease in MMP9 level in U0126 treated human cancer cell lines MCF-7 and MDA-MB-231, even more than what was caused by PD98059 (Moulik et al., 2014). This suggests enormous inhibitory potency of this non-competitive inhibitor in therapies.

The representative figures of the tumors (control and treated) are shown in Figure 10 which shows a larger tumor growth in most of the Control mice. Figure 11(A and B) displays the representative images of expression and activity of ERK 1/2 in Control and Drug treated set of mice. The Image J graphs accompanying the western blots clearly shows the sharp decrease in both expression and activity of ERK1/2 in Drug treated mice. Figure 12 A shows the representative zymograms of MMP9 and MMP2 in Mouse xenografts (Control and Drug treated) where there is a 3-4-fold decrease in the levels of both MMP 9 and MMP2 in most of the samples. Figure 12 B displays the zymograms of MMP 9 and MMP2 of blood serum from Control and drug treated mice. The results correspond the sharp decrease of the levels of active MMP 9 and MMP 2 in drug treated mice with respect to the control set. Pro-active form of MMP9 was clearly visible in most of the control set whereas it was diminished to the basal level in Drug treated mice. Representative images of RKIP, TIMP1 and TIMP2 in both Control and Drug treated mice xenografts are shown in Figure 13. In all the 42 samples RKIP was found to be low in Drug treated xenografts. In 33 samples TIMP1 and TIMP2 was found to be lower than Control sets.

Table 3 represents the parameters of the control group with respect to the treated group for statistical analysis. Test of proportion showed that the proportion of high values of ERK of the control group was significantly higher than the drug treated ( $p=0.001$ ). That was also higher for pERK ( $p=0.0001$ ), MMP9 ( $p=0.01$ ), MMP2 ( $p=0.01$ ), MMP 9 and MMP2 ( $p=0.01$ ). The values of TIMP1 ( $p=0.01$ ), TIMP2 ( $p=0.01$ ) and RKIP ( $p=.000001$ ) were found significantly lower.

Spearman's Rank Correlation by SPSS (version 20) showed that the values of ERK were significantly correlated with the values of MMP9 ( $p=0.00001$ ). Also the values of ERK were significantly correlated with the values of MMP2 ( $p=0.00001$ ). Statistical correlation of ERK was also shown with serum MMP9 ( $p=.0001$ ) and MMP 2( $p=.0001$ ). A highly significant negative correlation between ERK and TIMP 1 and TIMP2 were observed from the analysis ( $p=0.001$ ). Similarly, there was a highly significant negative correlation between values of ERK and RKIP ( $p=0.00001$ ).

The test revealed that the values of pERK were significantly correlated with the values of MMP9 ( $p=0.00001$ ) as well as MMP2 ( $p=0.00001$ ). Statistical correlation of pERK was also shown with serum MMP9 ( $p=.0001$ ) and MMP 2( $p=.0001$ ). A highly significant negative correlation between pERK and TIMP 1 ( $p=0.0001$ ) and TIMP2 ( $p=0.001$ ) were observed from the analysis. Similarly, there was a highly significant negative correlation between values of pERK and RKIP ( $p=0.001$ ).

Figure 14 are representative images showing expression of MMP 2, MMP9, ERK and pERK by immunohistochemistry of excised tumor cross-sections. There was a clear visibility of pERK in the Drug treated xenografts with respect to Control. ERK, MMP9 and MMP2 also corresponded similar expression levels in Drug treated xenografts. A routinely processed tumor section without the primary antibody served as negative control at each staining series.

Figure 15 displays representative examples of lungs and quantitative evaluation of macroscopically detectable lung metastases where the drug treated group showed a lower number of lung metastasis with respect to the control group.

Table 4 represents the distribution of lung metastasis according to tumor sizes. Test of proportion showed that proportion of lung metastasis for tumor size  $> 5 \text{ cm}^3$  was significantly lower in drug treated group compared to control group ( $p=0.001$ ). The proportion of lung metastasis for tumor size  $> 5 \text{ cm}^3$  was significantly lower in drug treated group compared to control group ( $p=0.001$ ).

Since most of the lung metastasis in the control group were for the tumor size  $> 5 \text{ cm}^3$ , there was no lung

metastasis in control group for tumor size  $< 1 \text{ cm}^3$ . Thus, though there was no significant difference in proportion of lung metastasis for tumor size  $< 1 \text{ cm}^3$  in both the groups ( $p=0.06$ ), the drug had significantly reduced the number of lung metastasis.

The proportion lung metastasis (36/38) for control group was significantly higher than the drug treated group (2/38) for the tumor size  $> 5 \text{ cm}^3$  ( $p=0.0001$ ). The effect of ERK Inhibitors and ERK siRNA on downstream and upstream molecules of ERK 1/2 is illustrated in Figure 16. Fn induced B16F10 cells showed an increase in the activity and expression of RKIP levels with respect to the controls which went up when treated with Inhibitors. Treatment of siRNA considerably elevated the levels of expression and activity of RKIP. Fn induced B16F10 cells showed a decrease in the activity of MEK1/2 levels with respect to the controls which went down when treated with Inhibitors. Treatment of siRNA did not alter the levels of expression or activity of MEK 1/2. The levels of p-cFOS and cFOS decreased appreciably when treated with ERK1/2 siRNA with respect to other sets.

Figure 17 demonstrates the levels of integrin molecules when ERK 1/2 is modulated. The intensity of alpha 5 integrin dropped considerably with the treatment of Inhibitor PD95059 and ERK siRNA in Fn treated B16F10 cells with respect to non- treated FN induced cells. U0126 treatment didn't show any change. Beta 1 integrin levels showed a similar decrease in the Inhibitor PD95059 and ERK siRNA treated cells. There was a considerable reduction in the pFAK levels in ERK1/2 siRNA treated cells, though the total protein levels of FAK remained unaltered. The levels of Paxillin also corresponded a similar pattern with a decrease in siRNA treated cells. The levels of TIMP1 got upregulated in Fn induced cells with respect to control which went up when PD9059 and U0126 were administered. The administration of ERK1/2 siRNA also elevated the levels of TIMP1 more than Control cells.

The activity and expression of expression of ERK1/2 being the main focus of this article offers a deep insight of the cell signaling scenario with respect to Integrin biology. The role of ERK1/2 in cell invasiveness has been elucidated in many recent evidences. The activity of MMP9 when treated with 20ug Fibronectin was considerably higher than the control cells and hence was taken as the standard of activation in our model. The dose dependent activity of MMP9 also showed a dose dependent increase in the expression of pERK1/2 which first indicated a possible role of pERK in the activation of MMP9. Also this increase was not consistent with the total protein levels of ERK and hence there was a hint that the change was due to the activity of the ERK protein. To see the possible role of pERK in MMP9 in MMP9 activity, MEK/ERK Inhibitor PD98509 was administered and the results showed a visible decrease in the activity of MMP9 correlated with the decrease of pERK when seen by zymogram. The depletion of ERK levels was only visible in the phosphor-protein form. There was hardly any visible change in the activity and expression PI-3K that was checked to see whether the inhibitor has an effect on other cell signaling molecules. This actually might show that there can be a role of ERK on the activity of MMP9. When another specific inhibitor U0126 was used, the activity of pERK1/2 got reduced appreciably supporting the role of ERK in regulating MMP9, which also got reduced likewise. To investigate more into the role of ERK, siRNA of ERK1/2 was administered and activity of MMP9 went almost beyond detection limit. This might show a possible correlation between Fn dependent MM9 activation and ERK. To check the migration of B16F10 cells with respect to ERK inhibition cells were treated respectively with PD9059, U0126 and ERK1/2 siRNA. The result indicated that the cell migration got markedly reduced after targeted inhibition by siRNA showing that ERK may have a role on cell adhesion molecules. This is in accordance with many recent evidences (Hunter et al., 2022).Evidences from the cell invasion assay also indicated that specific ERK modulation can actually change cell invasion rate suggesting an ERK

dependent ECM theory (Samson et al., 2022).

To analyze more about the role of ERK, mice model was introduced. When Statistical tests were performed between control and contralateral sets of tumor samples, the control values of pERK, ERK, MMP9, MMP2 were all significant compared to contralateral suggesting that the increase in activity of pERK or ERK simultaneous with MMP2 and MMP9 can have an inter-relation between them. To investigate deep into this matter more mouse model experiments were designed where U0126 inhibitor was treated. The gradual increase of tumor volume in control mice indicated that ERK modulation by the inhibitor lowered the tumor growth rate. Statistical analysis with test of proportion also corresponded that the drug has reduced the tumor size. The western blots representing the declining expression and activity of ERK1/2 along with MMP 9 and MMP 2 in drug treated mice also proves the role of ERK in modulating MMPs, which are regarded as markers in cancer progression. Spearman's rank correlation showed that ERK was significantly co-related with MMP2 and MMP9 both in serum and tissue samples. The results of RKIP TIMP1 and TIMP2 also suggested that there was a significant negative correlation between those molecules and ERK. All these results correspond to many recent evidences (Guo et al., 2006; Zhang et al., 2022). The images of IHC also showed the presence of ERK in control mouse xenografts. There was no change in the levels of ERK protein in liver and brain showing that normal ERK activity was not hampered due to the drug treatment. Cancer metastasis is an important phenomenon, which corresponds to the tumor virulence and is a vital indicator of the lethality of the disease. When test of proportion was introduced to see the distribution of lung metastasis according to tumor sizes, the proportion of lung metastasis for tumor size greater than 5cm<sup>3</sup> was lower in drug treated group compared to control group. This along with the quantitative evaluation of detectable lung metastasis showed that the drug significantly reduced lung metastasis, which might prove the possible role of ERK in cancer metastasis. These results gave us a possible effect of ERK modulation in an animal system and gave us an indication that melanoma might be restricted with ERK inhibition. In order to further investigate the possible upstream and downstream signaling of ERK1/2 and its relation with extra cellular matrix, B16F10 cells were again chosen. The levels of expression and activity of RKIP suggested that specific inhibition of ERK elevates the expression and activity of RKIP, which again suggests a possible feedback mechanism. This is in parallel to many recent evidences, which shows RKIP as a negative regulator of ERK (Cessna et al., 2022; Tang et al., 2010). Specific inhibition of ERK by siRNA does not alter the expression and activity of MEK1/2 showing that targeted ERK modulation may result in better treatment of melanoma. The decreased levels of cFOS indicated that transcription regulation downstream of ERK might be through cFOS.

The intensity of  $\alpha 5$  integrin,  $\beta 1$  integrin decreased markedly with ERK inhibition suggesting that ERK may have a role in directly modulating ECM. The marked reduction in the activity of FAK and Paxillin also supported this theory (Murillo et al., 2004; Teranishi et al., 2009). Fn induced cells also showed elevated levels of TIMP1 when ERK was inhibited suggesting the further role of ERK in MMP9 modulation.

Overall, the role of ERK in melanoma with respect to components of ECM was highlighted in this study. Evidences which suggested that ERK is involved in regulating proteolytic enzymes like MMP9 that degrade the basement membrane also stand true in this study. The study provides a deep insight in the mechanism of ERK regulation which can be further used in diagnostic and therapeutic interventions after clinical validation.

## ACKNOWLEDGEMENT

The authors acknowledge Department of Science and Technology, India and Suraksha Diagnostics Pvt. Ltd, Kolkata for all the support regarding the study.

## CONFLICT OF INTEREST

The authors show no conflict of interest

## REFERENCES

1. Barkan, D., Kleinman, H., Simmons, J.L., Asmussen, H., Kamaraju, A.K., Hoenorhoff, M.J., Liu, Z., Costes, S. V, Cho, E.H., Lockett, S., Khanna, C., Chambers, A.F., Green, J.E., 2008. Inhibition of Metastatic Outgrowth from Single Dormant Tumor Cells by Targeting the Cytoskeleton 6241–6251. <https://doi.org/10.1158/0008-5472.CAN-07-6849>
2. Bessard, A., Frémin, C., Ezan, F., Fautrel, A., Gailhouste, L., Baffet, G., 2008. RNAi-mediated ERK2 knockdown inhibits growth of tumor cells in vitro and in vivo. *Oncogene* 27, 5315–5325. <https://doi.org/10.1038/onc.2008.163>
3. Braeuer, R.R., Watson, I.R., Wu, C.J., Mobley, A.K., Kamiya, T., Shoshan, E., Bar-Eli, M., 2014. Why is melanoma so metastatic? *Pigment Cell Melanoma Res.* 27, 19–36. <https://doi.org/10.1111/pcmr.12172>
4. Cao, Y., Liu, X., Lu, W., Chen, Y., Wu, X., Li, M., Wang, X., Zhang, F., Jiang, L., Zhang, Y., Hu, Y., Xiang, S., Shu, Y., Bao, R., Li, H., Wu, W., Weng, H., Yen, Y., Liu, Y., 2015. Fibronectin promotes cell proliferation and invasion through mTOR signaling pathway activation in gallbladder cancer. *Cancer Lett.* 1–10. <https://doi.org/10.1016/j.canlet.2015.01.041>
5. Caunt, C.J., Sale, M.J., Smith, P.D., Cook, S.J., 2015. MEK1 and MEK2 inhibitors and cancer therapy: the long and winding road. *Nat. Publ. Gr.* 15, 577–592. <https://doi.org/10.1038/nrc4000>
6. Cessna, H., Baritaki, S., Zaravinos, A., Bonavida, B., 2022. The Role of RKIP in the Regulation of EMT in the Tumor Microenvironment. *Cancers (Basel).* 14, 1–35. <https://doi.org/10.3390/cancers14194596>
7. Chung, Y.C., Hyun, C., 2020. Inhibitory Effects of Pinostilbene Hydrate on Melanogenesis in B16F10 Melanoma Cells via ERK and p38 Signaling Pathways 1–12.
8. Czarnecka, A.M., Bartnik, E., Fiedorowicz, M., Rutkowski, P., 2020. Targeted therapy in melanoma and mechanisms of resistance. *Int. J. Mol. Sci.* 21, 1–21. <https://doi.org/10.3390/ijms21134576>
9. Das, S., Banerji, A., Frei, E., Chatterjee, A., 2008. Rapid expression and activation of MMP-2 and MMP-9 upon exposure of human breast cancer cells ( MCF-7 ) to fibronectin in serum free medium 82, 467–476. <https://doi.org/10.1016/j.lfs.2007.12.013>
10. Eble, J.A., Niland, S., 2019. The extracellular matrix in tumor progression and metastasis. *Clin. Exp. Metastasis* 36, 171–198. <https://doi.org/10.1007/s10585-019-09966-1>
11. Ebner, H.L., Blatzer, M., Nawaz, M., Krumschnabel, G., 2007. Activation and nuclear translocation of ERK in response to ligand-dependent and -independent stimuli in liver and gill cells from rainbow trout 1036–1045. <https://doi.org/10.1242/jeb.02719>
12. Elgundi, Z., Papanicolaou, M., Major, G., Cox, T.R., Melrose, J., Whitelock, J.M., Farrugia, B.L., 2020. Cancer Metastasis: The Role of the Extracellular Matrix and the Heparan Sulfate Proteoglycan Perlecan. *Front. Oncol.* 9. <https://doi.org/10.3389/fonc.2019.01482>
13. Guo, L.J., Luo, X.H., Xie, H., Zhou, H.D., Yuan, L.Q., Wang, M., Liao, E.Y., 2006. Tissue

- inhibitor of matrix metalloproteinase-1 suppresses apoptosis of mouse bone marrow stromal cell line MBA-1. *Calcif. Tissue Int.* 78, 257–270. <https://doi.org/10.1007/s00223-005-0092-x>
14. Haass, N.K., Smalley, K.S.M., Li, L., Herlyn, M., 2005. Adhesion, migration and communication in melanocytes and melanoma. *Pigment Cell Res.* 18, 150–159. <https://doi.org/10.1111/j.1600-0749.2005.00235.x>
  15. Hackl, N., Klemis, V., Nakchbandi, I.A., 2021. Inhibition of fibronectin accumulation suppresses tumor growth. *Neoplasia* 23, 837–850. <https://doi.org/10.1016/j.neo.2021.06.012>
  16. He, J., Xie, N., Yang, J., Guan, H., Chen, W., Wu, H., Yuan, Z., Wang, K., Li, G., Sun, J., Yu, L., 2014. siRNA-mediated suppression of synuclein  $\gamma$  inhibits MDA-MB-231 cell migration and proliferation by downregulating the phosphorylation of AKT and ERK. *J. Breast Cancer* 17, 200–206. <https://doi.org/10.4048/jbc.2014.17.3.200>
  17. Hunter, E.J., Hamaia, S.W., Kim, P.S.K., Malcor, J.D.M., Farndale, R.W., 2022. The effects of inhibition and siRNA knockdown of collagen-binding integrins on human umbilical vein endothelial cell migration and tube formation. *Sci. Rep.* 12, 1–13. <https://doi.org/10.1038/s41598-022-25937-1>
  18. Invasiveness, T., Cell, C., 2014. *Journal of Tumor* 2, 87–98. <https://doi.org/10.6051/j.issn.1819-6187.2014.02.20>
  19. Kim, S.H., Turnbull, J., Guimond, S., 2011. Extracellular matrix and cell signalling: The dynamic cooperation of integrin, proteoglycan and growth factor receptor. *J. Endocrinol.* 209, 139–151. <https://doi.org/10.1530/JOE-10-0377>
  20. Kohno, M., Pouyssegur, J., 2009. *Annals of Medicine Targeting the ERK signaling pathway in cancer therapy* 3890. <https://doi.org/10.1080/07853890600551037>
  21. Kumar, S., Sunita, S., Padhan, J., Jangde, N., Ray, R., Rai, V., 2020. MYH9 suppresses melanoma tumorigenesis, metastasis and regulates tumor microenvironment. *Med. Oncol.* 1–10. <https://doi.org/10.1007/s12032-020-01413-6>
  22. Malemud, C.J., 2006. Department of Medicine, Division of Rheumatic Diseases and Department of Anatomy, Case Western Reserve University School of Medicine, Cleveland, Ohio 1696–1701.
  23. Marampon, F., Bossi, G., Ciccarelli, C., Rocco, A. Di, Sacchi, A., Pestell, R.G., Zani, B.M., 2009. MEK / ERK inhibitor U0126 affects in vitro and in vivo growth of embryonal rhabdomyosarcoma 671, 543–552. <https://doi.org/10.1158/1535-7163.MCT-08-0570>
  24. Mayes, P.A., Degenhardt, Y.Y., Wood, A., Toporovskya, Y., Diskin, S.J., Haglund, E., Moy, C., Wooster, R., Maris, J.M., 2013. Mitogen-activated protein kinase (MEK/ERK) inhibition sensitizes cancer cells to centromere-associated protein e inhibition. *Int. J. Cancer* 132. <https://doi.org/10.1002/ijc.27781>
  25. Merchant, M., Moffat, J., Schaefer, G., Chan, J., Wang, X., Orr, C., Cheng, J., Hunsaker, T., Shao, L., Wang, S.J., Wagle, M.C., Lin, E., Haverty, P.M., Shahidi-Latham, S., Ngu, H., Solon, M., Eastham-Anderson, J., Koeppen, H., Huang, S.M.A., Schwarz, J., Belvin, M., Kirouac, D., Junttila, M.R., 2017. Combined MEK and ERK inhibition overcomes therapy-mediated pathway reactivation in RAS mutant tumors. *PLoS One* 12, 1–22. <https://doi.org/10.1371/journal.pone.0185862>
  26. Murillo, C.A., Rychahou, P.G., Evers, B.M., 2004. Inhibition of  $\alpha 5$  integrin decreases PI3K activation and cell adhesion of human colon cancers. *Surgery* 136, 143–149. <https://doi.org/10.1016/j.surg.2004.04.006>
  27. Paul, C.D., Mistriotis, P., Konstantopoulos, K., 2016. migration in confined spaces. *Nat. Publ. Gr.* <https://doi.org/10.1038/nrc.2016.123>
  28. Reffay, M., Parrini, M.C., Ladoux, B., Buguin, A., Coscoy, S., Amblard, F., Camonis, J., 2014. A

- RT I C L E S Interplay of RhoA and mechanical forces in collective cell migration driven by leader cells  
16. <https://doi.org/10.1038/ncb2917>
29. Samson, S.C., Khan, A.M., Mendoza, M.C., 2022. ERK signaling for cell migration and invasion 1–9. <https://doi.org/10.3389/fmolb.2022.998475>
30. Sen, T., Dutta, A., Maity, G., Chatterjee, A., 2010. Fibronectin induces matrix metalloproteinase-9 (MMP-9) in human laryngeal carcinoma cells by involving multiple signaling pathways. *Biochimie* 92, 1422–1434. <https://doi.org/10.1016/j.biochi.2010.07.005>
31. Sengupta, S., Parent, C.A., Bear, J.E., 2022. The principles of directed cell migration 22, 529–547. <https://doi.org/10.1038/s41580-021-00366-6>.The
32. Shain, A.H., Bastian, B.C., 2016. From melanocytes to melanomas. *Nat. Rev. Cancer* 16, 345–358. <https://doi.org/10.1038/nrc.2016.37>
33. Shin, S.Y., Sun, S.O., Ko, J.Y., Oh, Y.S., Cho, S., Park, D., Park, K.M., 2020. New Synthesized Galloyl-RGD Inhibits Melanogenesis by Regulating the CREB and ERK Signaling Pathway in B16F10 Melanoma Cells 1–11. <https://doi.org/10.1111/php.13277>
34. Song, Y., Bi, Z., Liu, Y., Qin, F., Wei, Y., Wei, X., 2022. Targeting RAS–RAF–MEK–ERK signaling pathway in human cancer: Current status in clinical trials. *Genes Dis.* 1–13. <https://doi.org/10.1016/j.gendis.2022.05.006>
35. Sugiura, R., Satoh, R., Takasaki, T., 2021. Erk: A double-edged sword in cancer. erk-dependent apoptosis as a potential therapeutic strategy for cancer. *Cells* 10. <https://doi.org/10.3390/cells10102509>
36. Tang, H., Park, S., Sun, S.C., Trumbly, R., Ren, G., Tsung, E., Yeung, K.C., 2010. RKIP inhibits NF- $\kappa$ B in cancer cells by regulating upstream signaling components of the I $\kappa$ B kinase complex. *FEBS Lett.* 584, 662–668. <https://doi.org/10.1016/j.febslet.2009.12.051>
37. Tanimura, S., Asato, K., Fujishiro, S., Kohno, M., 2003. Specific blockade of the ERK pathway inhibits the invasiveness of tumor cells: down-regulation of matrix metalloproteinase-3/-9/-14 and CD44 304, 801–806. [https://doi.org/10.1016/S0006-291X\(03\)00670-3](https://doi.org/10.1016/S0006-291X(03)00670-3)
38. Tanimura, S., Takeda, K., 2017. JB Review ERK signalling as a regulator of cell motility 162, 145–154. <https://doi.org/10.1093/jb/mvx048>
39. Teranishi, S., Kimura, K., Nishida, T., 2009. Role of formation of an ERK-FAK-paxillin complex in migration of human corneal epithelial cells during wound closure in vitro. *Investig. Ophthalmol. Vis. Sci.* 50, 5646–5652. <https://doi.org/10.1167/iovs.08-2534>
40. Virginia, W., 2019. cro WNT1-inducible signaling pathway protein 1 ( WISP1 / CCN4 ) stimulates melanoma invasion and metastasis by promoting the epithelial – mesenchymal transition 1, 5261–5280. <https://doi.org/10.1074/jbc.RA118.006122>
41. Winkler, J., Abisoye-Ogunniyan, A., Metcalf, K.J., Werb, Z., 2020. Concepts of extracellular matrix remodelling in tumour progression and metastasis. *Nat. Commun.* 11, 1–19. <https://doi.org/10.1038/s41467-020-18794-x>
42. Yan, Z., Ohuchida, K., Fei, S., Zheng, B., Guan, W., Feng, H., Kibe, S., Ando, Y., Koikawa, K., Abe, T., Iwamoto, C., Shindo, K., Moriyama, T., Nakata, K., Miyasaka, Y., Ohtsuka, T., Mizumoto, K., Hashizume, M., Nakamura, M., 2019. Inhibition of ERK1 / 2 in cancer-associated pancreatic stellate cells suppresses cancer – stromal interaction and metastasis 8, 1–16.
43. Zhang, G., Luo, X., Wang, Z., Xu, J., Zhang, W., Chen, E., Meng, Q., Wang, D., Huang, X., Zhou, W., Song, Z., 2022. TIMP-2 regulates 5-Fu resistance via the ERK/MAPK signaling pathway in colorectal cancer. *Aging (Albany. NY).* 14, 297–315. <https://doi.org/10.18632/aging.203793>